Proper-Time Resolution Modelling

July 2, 2007

Abstract

The paper reports on a study of the resolution of the proper-time of the B^0 and B^+ mesons. The decay modes used are $B^+ \to J/\psi(\mu^+\mu-)K^+$ and $B^0 \to J/\psi(\mu^+\mu-)K^*(K^+\pi-)$ and their conjugates. A resolution model based on the proper-time residuals and the corresponding per-event error is proposed and results are presented on the two decay modes studied. While the model still requires further refinement the approach presented appears promising.

LHCb Public Note

Issue	Final
Reference	LHCb 2007-055
Created	January 10, 2007
Last Modified	July 2, 2007

Prepared by P. Vankov, G. Raven
NIKHEF, Amsterdam, The Netherlands

Contents

1 Introduction **3**

2 Software and Data **4**

3 Event selection **4**

4 Resolution Model **9**
4.1 Proper-time reconstruction 9
4.2 Resolution model 10
4.3 The Per-event-errors 12
4.4 Determination of the Resolution Model Parameters 12
4.5 Validation of the model 16

5 Determination of the parameters on real data **22**
5.1 Method 22
5.2 Results 23

6 Dependence on t_{true} **26**
6.1 Test for dependence on t_{true} 26
6.2 Explanation of the t_{true} dependence 29
6.3 Primary Vertex re-definition 33
6.3.1 The resolution model parameters after the update of the PV 39

7 Summary and conclusions **41**

1 Introduction

The main goal of the study presented here is to derive a reliable *resolution model*, which is able to describe with sufficient precision the distribution of the decay time residuals: $t^i_{rec} - t^i_{true}$, taking into account the B mesons proper-time per-event-errors, $\sigma^i_{t_{rec}}$, measured with the LHC*b* experiment. The resolution of the proper-time is an important ingredient in the measurement of time-dependent (CP) asymmetries, especially in the decay of the rapidly oscillating B_s meson. Thereby we need to model as well as possible its behaviour.
In this note we propose a model for the decay time resolution. The parameters of this model are first determined using Monte-Carlo simulation truth information for $t^i_{rec} - t^i_{true}$. Then, later in this note, the parameters are determined in a manner that can be applied to real data using t^i_{rec} and $\sigma^i_{t_{rec}}$.
To perform the study we have chosen to analyze two *b*-flavored mesons: B^+ and B^0. The B^+ is selected and reconstructed in the mode: $B^+ \to J/\psi(1S)K^+$, where $J/\psi(1S)$ decays in its turn into μ^+ and μ^-. The B^0 meson is reconstructed in the mode: $B^0 \to J/\psi(1S)K^*(892)$, with $J/\psi(1S) \to \mu^+\mu^-$, and $K^*(892) \to K^+\pi^-$. The complex conjugated modes are also considered[1]. Both B mesons decay weakly through a tree-level diagram, as is shown in Fig.1.

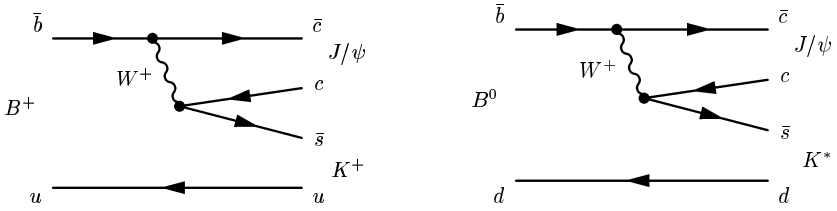

Figure 1: *Feynman diagrams for the exploited channels.*

The reason to explore these particular channels is two-fold:

- Among the interesting B meson decay channels, these channels have the highest expected annual signal yield [1]. The high event statistics ensures fast data collection. Therefore the two decay modes will be among the first ones to be reconstructed once the LHC*b* detector is operational.

- The two channels are efficiently triggered and selected due to the presence of the di-muon pair. As a result, there is no need for impact parameter cuts which distort the proper-time distribution.

[1] $B^- \to J/\psi(1S)K^-$ with $J/\psi(1S) \to \mu^+\mu^-$ and $\overline{B^0} \to J/\psi(1S)\overline{K^*(892)}$ with $J/\psi(1S) \to \mu^+\mu^-$, $\overline{K^*(892)} \to K^-\pi^+$; Unless otherwise noted, charge conjugated modes are also implicitly considered throughout this note.

As a result, these channels are expected to be excellent *control channels* to study the detector response, and to obtain a resolution model which, hopefully, can also be used for other B meson decay modes.

The note is organized as follows:
Section 2 contains a brief description of the software framework and the data set used. In Sec. 3 the method to select $B^+ \to J/\psi K^+$ and $B^0 \to J/\psi K^*$ is discussed. In Sec. 4 the construction of a resolution model is presented and applied to the data. The determination of the resolution model parameters on *real* data is described in Sec. 5 and results are presented. Section 6 focuses on the discovered effect of dependence of the resolution model on the true proper-time t_{true}. An explanation of the effect is given and a way to resolve it is proposed. The solution is based on a redefinition of the primary vertex (PV) position by exclusion of the *B* decay products from the PV reconstruction. The note finishes in Sec. 7 with summary and conclusions.

2 Software and Data

The data that we used for our analysis is part of the so called Data Challenge 2004, also known as the DC'04 dataset. This dataset includes various event types, generated under the same conditions (detector description geometry, reconstruction algorithms, etc.). For the production of the data GAUSS [2] v15r8, BOOLE [3] v5r8 and BRUNEL [4] v23r7 are used, while DAVINCI [5] v12r18 is used for the selection and analysis. The files with the reconstructed data are stored at CERN in the form of DST files. These files are the input for the DAVINCI program. For the current study, only $B^+ \to J/\psi K^+$ and $B^0 \to J/\psi K^*$ signal samples are used. This implies that each event contains one B meson which decays into the signal modes. The effect of the inclusion of backgrounds will be part of a follow-up study.
About $2 \cdot 10^6$ signal[2] events were subject to selection and analysis.

3 Event selection

The topologies of $B^+ \to J/\psi K^+$ and $B^0 \to J/\psi K^*$, shown in Fig. 2 are similar, with one distinguishable secondary vertex - the B meson vertex.
The J/ψ and K^* resonances have extremely short life-times ($\sim 10^{-23}$ seconds) and hence do not generate displaced vertices with respect to their production point.

[2] A study including background events is ongoing at the time of writing.

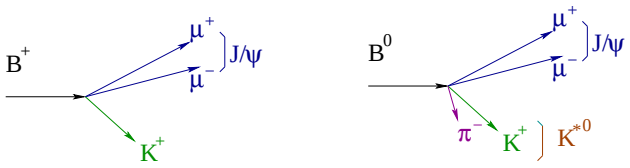

Figure 2: *Topologies for $B^+ \to J/\psi K^+$ and $B^0 \to J/\psi K^*$ decays.*

The events are selected and reconstructed by first reconstructing the $J/\psi(1S) \to \mu^+\mu^-$, then the $K^*(892) \to K^+\pi^-$, and finally the $B^+ \to J/\psi(1S)K^+$ and $B^0 \to J/\psi K^*$ mesons. Details are given below:

- The $J/\psi(1S)$ selection and reconstruction is identical for both channels. The $J/\psi(1S)$ candidates are reconstructed by combining two oppositely charged muons with $p_T > 1000$ MeV/c and requiring their invariant mass to be within a ± 50 MeV/c^2 window around the nominal $J/\psi(1S)$ mass. A quality criterion of $\chi^2 < 9$ for the J/ψ vertex fit is required.

$B^+ \to J/\psi(1S)K^+$ decay:

- The B^+ candidates are reconstructed on the base of the selected J/ψ candidates and charged kaons with $p_T > 2000$ MeV/c. The B^+ candidate invariant mass is required to be within a ± 50 MeV/c^2 mass window around the nominal B^+ mass, see Fig. 3. A quality criterion of $\chi^2 < 20$ for the B^+ vertex fit is applied.

$B^0 \to J/\psi(1S)K^*(892)$ decay:

- The $K^*(892)$ candidates are reconstructed from the identified K^+ and π^-. The $K^*(892)$ candidate must have a $p_T > 1000$ MeV/c, and its invariant mass is required to be within a ± 150 MeV/c^2 window around the $K^*(892)$ mass. A quality criterion of $\chi^2 < 9$ for the vertex fit is required.

- The B^0 candidates are reconstructed based on the selected J/ψ and the selected K^* candidates. The invariant mass of the B^0 candidate is required to be within ± 50 MeV/c^2 of the expected B^0 mass, see Fig. 4. A quality criterion of $\chi^2 < 27$ for the B^0 vertex fit is applied.

Given that the expected signal yield is expected to be a limiting factor, we decided to keep our selection procedure simple and accept only those events which contain a single reconstructed B candidate. At the price of losing data by rejecting higher multiplicity events, we achieve better selection stability and a decreased

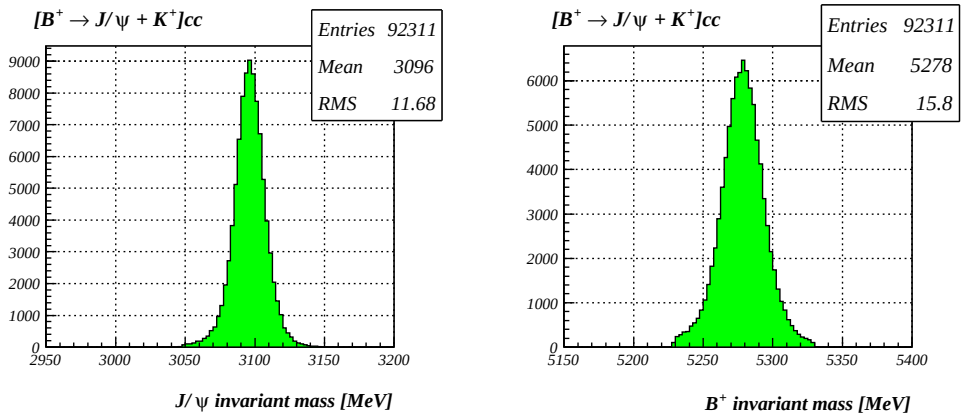

Figure 3: *The reconstructed invariant mass distribution for* $J/\psi(1S) \rightarrow \mu^+\mu^-$ *and for* $B^+ \rightarrow J/\psi K^+$

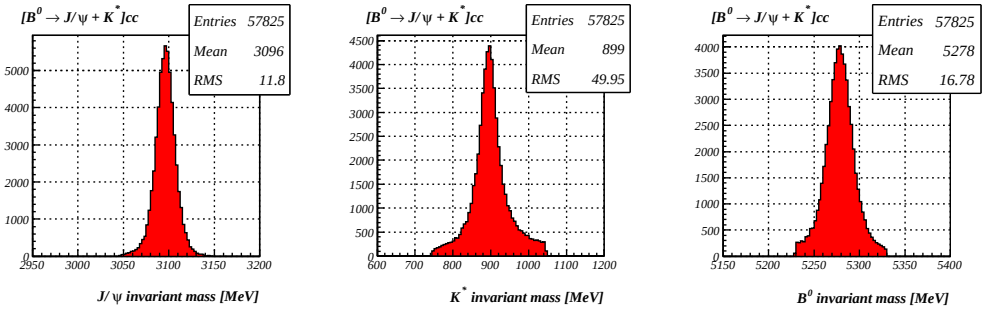

Figure 4: *The reconstructed invariant mass distribution for* $J/\psi(1S) \rightarrow \mu^+\mu^-$, *for* $K^* \rightarrow K^+\pi^-$ *and for* $B^0 \rightarrow J/\psi(1S)K^*(892)$

channel	*# Generated Events*	*# Selected Events*
$B^+ \to J/\psi K^+$	684000	92311
$B^0 \to J/\psi K^*$	960000	57825

Table 1: *Event Selection - Results.*

number of mis-reconstructed B candidates. The results from the event selection are summarized in Table 1.
To check whether the selection introduces a bias on the proper-time distribution, we have plotted the Monte-Carlo true proper decay time for both channels and fitted this with the expected exponential distribution $e^{\Gamma_B t_{true}}$, as shown in Fig. 5 and Fig. 6. It is apparent that no large bias is present and the proper-time acceptance is flat to a good approximation. The values of the mean B lifetimes $\tau_B = -1/\Gamma_B$ are extracted from the fits and should match with the input MC values, see Table 2.

MC inputs	*Fit outputs*
$\tau_{B^+}^{MC} = 1.671$ [ps]	$\tau_{B^+} = 1.695 \pm 0.006$ [ps]
$\tau_{B^0}^{MC} = 1.536$ [ps]	$\tau_{B^0} = 1.523 \pm 0.006$ [ps]

Table 2: B^+ *and* B^0 *mean lifetimes.*

The small discrepancy we observe is not completely understood, but could be a hint of a small bias in either in the event selection itself or in its inputs, *e.g.* the reconstruction efficiencies.
To indicate the quality of the exponential fit of the true proper-times in Fig. 5 and Fig. 6, the fit *Residuals* and the fit *Pulls* are given.
The *Residual* and *Pull* from the fit are defined as:

$$Residual(t_{true}) = \text{data}(t_{true}) - \text{fit}(t_{true}) \tag{1}$$

$$Pull(t_{true}) = \frac{\text{data}(t_{true}) - \text{fit}(t_{true})}{\text{data}(t_{true})_{error}} \tag{2}$$

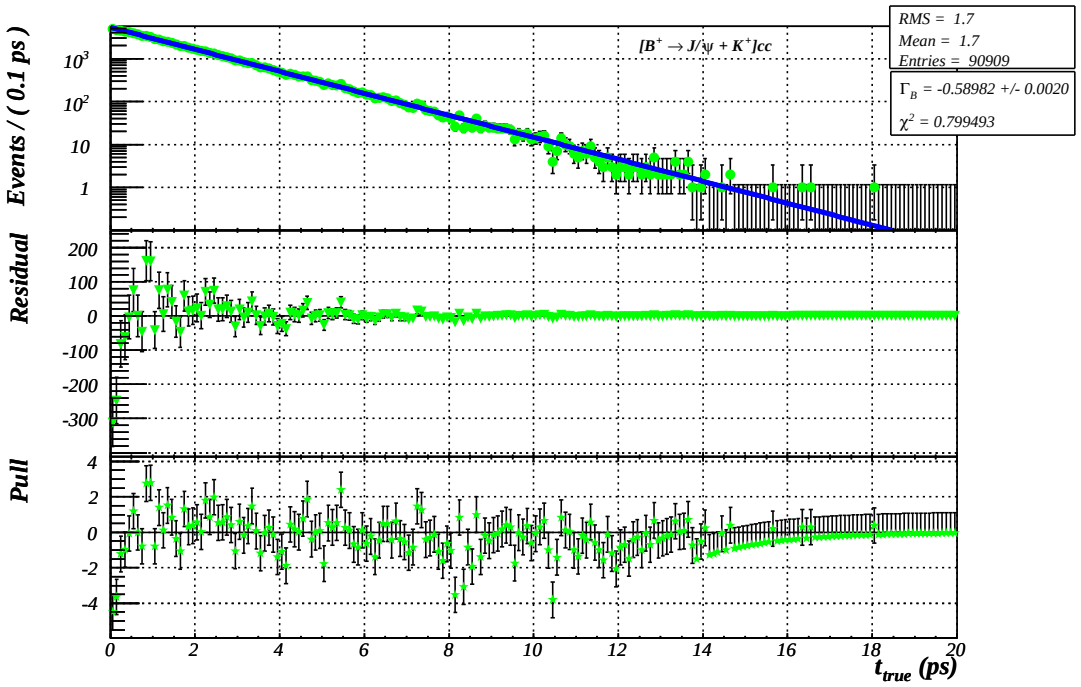

Figure 5: *The MC true proper decay times fitted exponentially, with the corresponding fit residuals and pulls for channel* $B^+ \to J/\psi(1S)K^+$.

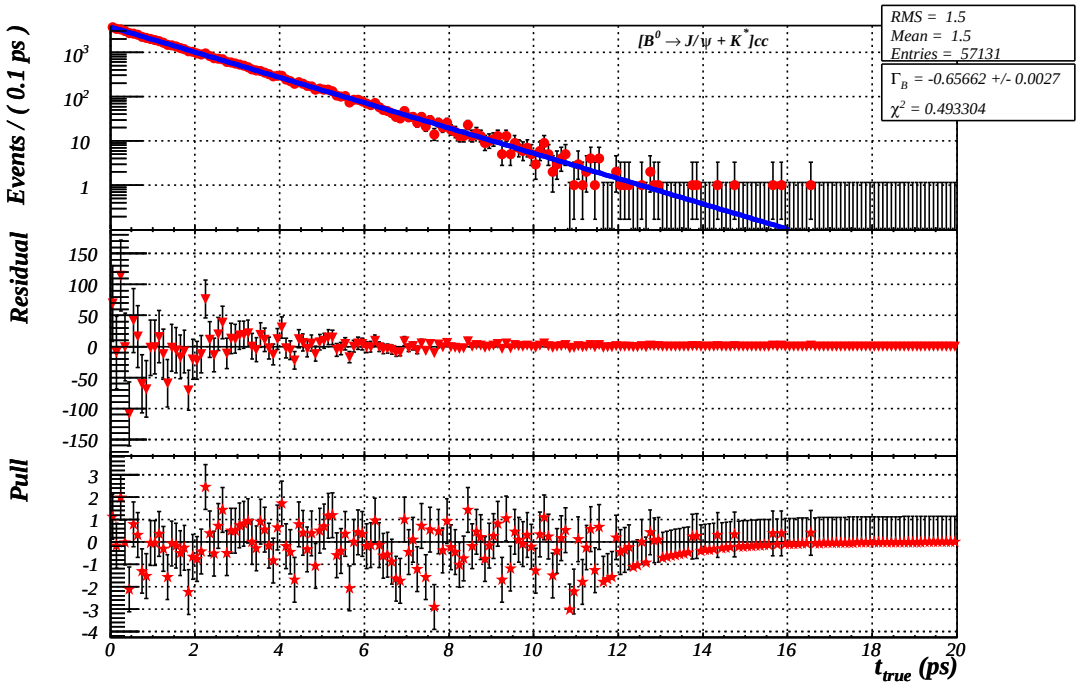

Figure 6: *The MC true proper decay times fitted exponentially, with the corresponding fit residuals and pulls for channel* $B^* \to J/\psi(1S)K^*$.

4 Resolution Model

The aim of this section is to describe in details the modelling of the resolution model and its ingredients. It is divided in 5 subsections. In Sec. 4.1 the reconstruction of the proper-time is presented. The basic resolution model is derived in Sec. 4.2. Section 4.3 shows how the proper-time per-event errors are included in this model. Next, the determination of how the parameters of the model depend on these per-event errors is explained in Sec. 4.4. The final subsection, Sec. 4.5, describes how the parameters of the resolution model are obtained using an unbinned maximum likelihood fit.
The main software packages used in our analysis are ROOFIT [8] - a tool for modelling the expected distribution of events in a physics analysis and ROOT [9] - a data analysis framework.

4.1 Proper-time reconstruction

The reconstructed proper-time of a B candidate t_{rec}, together with the estimated error, is obtained from a constrained χ^2 fit described in [6]. Ingredients of the fit are the measured primary vertex position $\vec{x}$ (the production point), the measured decay vertex position $\vec{v}$ and the measured momentum $\vec{p}$ of the B meson. These nine observables, $\mathcal{O} = (\vec{v}, \vec{p}, \vec{x})$, are the input for the fit and, in the absence of detector resolution effects, are related by the following constraint:

$$\vec{x} = \vec{v} - t\frac{\vec{p}}{m} \ , \tag{3}$$

where t is the B proper-time.
As a result, seven parameters $\mathcal{P}$ are needed to describe the system: the three components of the reconstructed decay point $\vec{\tilde{x}}$, the reconstructed momentum $\vec{\tilde{p}}$ and the reconstructed proper-time t_{rec}, $\mathcal{P} = (\vec{\tilde{v}}, \vec{\tilde{p}}, t_{rec})$. It is assumed that the decay vertex and the particle are independent (i.e that none of the daughters of the particle were used in the determination of the primary production vertex). The seven parameters $\mathcal{P}$ are determined by minimizing the following χ^2:

$$\chi^2(\mathcal{P}) = \mathcal{R}^T W_{\mathcal{O}} \mathcal{R} \ , \tag{4}$$

where $\mathcal{R}$ are the residuals between the measurements $\mathcal{O}$ and their prediction based on the parameters $\mathcal{P}$, and $W_{\mathcal{O}}$ is the weight matrix corresponding to the observables $\mathcal{O}$. $W_{\mathcal{O}}$ takes into account the correlation between $\vec{v}$ and $\vec{p}$ provided the vertex algorithm that determined $\vec{v}$ and $\vec{p}$ has computed this correlation. It is assumed that there is no correlation between $\vec{v}$ and $\vec{p}$ on the one hand, and $\vec{x}$ on the other. The errors on $\mathcal{P}$ are given by the second order derivatives of the χ^2 with respect to $\mathcal{P}$ at the minimum.

As the proper-time t_{rec} is one of the parameters $\mathcal{P}$, the fit, by construction, computes an error $\sigma_{t_{rec}}$ for each reconstructed B decay time - t_{rec}. As a result of this procedure, this error takes into account the specified correlations amongst the inputs. This error is called the proper-time per-event-error or simply the per-event-error. The distributions of the per-event-errors for our channels of interest are shown in Fig. 7. The B^0 decay mode has a smaller mean $\sigma_{t_{rec}}$ than the B^+ mode, which is most likely due to the fact that the B^0 vertex is reconstructed with four tracks, while the B^+ vertex is reconstructed with only three (see Fig. 2). As a result the position of the B^0 vertex is determined more precisely, hence the decay length is better defined and thus the proper-time uncertainty is smaller.

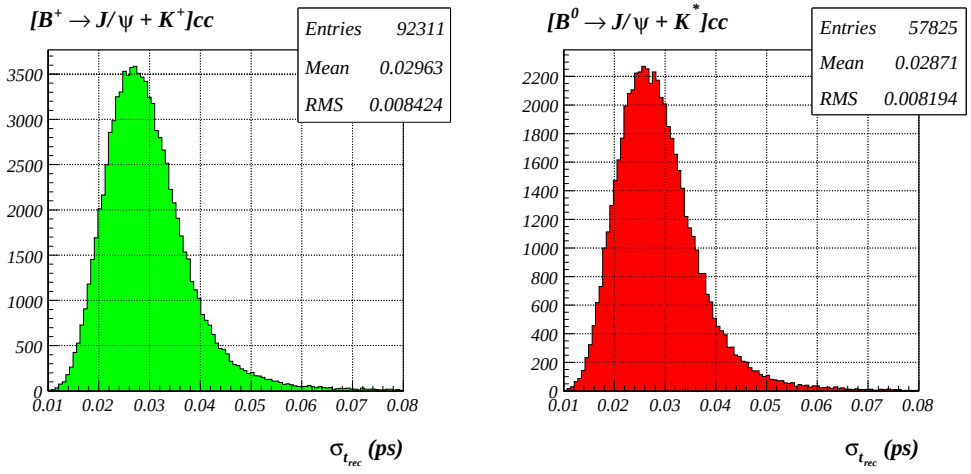

Figure 7: *Proper-time per-event-error distributions.*

In Sec. 6.3 we will refit the primary vertex, explicitly excluding the tracks originating from the B [3].

4.2 Resolution model

A proper-time resolution model $R(x)$ is a mathematical construction which describes the distribution of the decay time residuals: $x^i = t^i_{rec} - t^i_{true}$, taking into

[3]The tracks from the tagging B, or any other long-lived resonances, cannot explicitly be excluded as they are not fully reconstructed. However, the bias introduced by the possible inclusion of these tracks is modelled and determined implicitly, and as a result does not bias the measurements. This is fundamentally different from the case where tracks from the signal are (re)used in the primary vertex, an effect that is more likely for short-lived B mesons. In this case, the bias depends on the true proper-time t_{true}, and this is *not* modelled as it is at this point unknown how one would determine such a bias without knowledge of t_{true}, *i.e.* for real data.

account the per-event-errors. Ideally, with a perfectly described detector response, $R(x)$ is represented by a Gaussian:

$$R(t_{rec} - t_{true}, \sigma_{t_{rec}}) = \frac{e^{-\frac{1}{2}\left(\frac{t_{rec}-t_{true}}{\sigma_{t_{rec}}}\right)^2}}{\sqrt{2\pi}\sigma_{t_{rec}}} \tag{5}$$

However, in real life, the function $R(x)$ typically takes a more complicated form. In order to understand the detector response, we need to determine $R(x)$. Knowledge of $R(x)$, in combination with sufficiently good resolution, is a necessary ingredient for time-dependent CP asymmetry measurements given that the oscillation amplitude decreases when the resolution degrades.
A natural suggestion for a realistic $R(x)$ function is a sum of Gaussians with different fractions:

$$R(x = t_{rec} - t_{true}) = \frac{N}{\sqrt{2\pi}}\left[(1 - f_1)\frac{e^{-\frac{1}{2}\left(\frac{x-M_1}{S_1}\right)^2}}{S_1} + f_1\frac{e^{-\frac{1}{2}\left(\frac{x-M_2}{S_2}\right)^2}}{S_2}\right] , \tag{6}$$

where M_1, M_2 represent biases to the reconstructed time.
Our first try was based on an analysis using the model in Eq. (6). In due process we modified $R(x)$ into:

$$\begin{aligned} R(x = t_{rec} - t_{true}) = \frac{N}{\sqrt{2\pi}}\Bigg[&(1 - f_1 - f_2)e^{-\frac{1}{2}\left(\frac{x-M}{S}\right)^2} + f_2 e^{-\frac{1}{2}\left(\frac{x}{S_{fixed}}\right)^2} \\ &+ f_1\left(e^{-\frac{1}{2}\left(\frac{x}{S}\right)^2} \otimes e^{-\left(\frac{x}{\tau}\right)}\right)\Bigg] , \end{aligned} \tag{7}$$

which provides a better description of the observed residuals.
Now, $R(x)$ consists of three terms with different fractions defined by the fraction parameters: f_1 and f_2. The first term is a Gaussian of mean M and width S. The second term is a Gaussian of mean zero and width S_{fixed}, where S_{fixed} is not a free parameter but a fixed number, set to 10 ps, to describe the wide tails of the distribution. The third term is a Gaussian with mean 0 and sigma S convolved with an exponent with index $-\tau^{-1}$. This term is added to allow for a modified exponential decay time distribution. It describes the fact that there is a non negligible chance that the primary vertex position is biased in the downstream direction due to the inclusion of tracks from long(er) lived resonances, which cause a bias in the reconstructed proper-time towards smaller values. There are five free parameters in this model - $(M, S, f_1, f_2, \tau) = \vec{p}$. The question is how to determine these parameters.

4.3 The Per-event-errors

So far, constructing the resolution model we did not take into account the observed per-event-errors. In a perfect detector the width of the resolution function, for a given event, is expected to be determined by this per-event error. Accordingly, we make our model conditional on the per-event-error by substituting the width by the observed per-event error and by weighing it with a p.d.f. describing the per-event-errors - $P(\sigma_{t_{rec}})$:

$$\mathcal{R}(t_{rec} - t_{true}, \sigma_{t_{rec}}) = R(t_{rec} - t_{true} \mid \sigma_{t_{rec}}) \times P(\sigma_{t_{rec}}) \ . \tag{8}$$

The $P(\sigma_{t_{rec}})$ is constructed through a technique called *kernel estimation*, "KEYS". The best possible probability density function that aims to describe the $\sigma_{t_{rec}}$ parent distribution is obtained via a superposition of Gaussians, centered on the observed values. Note that this p.d.f. does not have any free parameters. For more details see Ref. [7]. The program implementation has been realized with the help of the ROOKEYSPDF class, which is a part of ROOFIT package.
The $\sigma_{t_{rec}}$ distributions are given in Fig. 8, superimposed with the p.d.f.'s $P(\sigma_{t_{rec}})$, as obtained with ROOKEYSPDF.

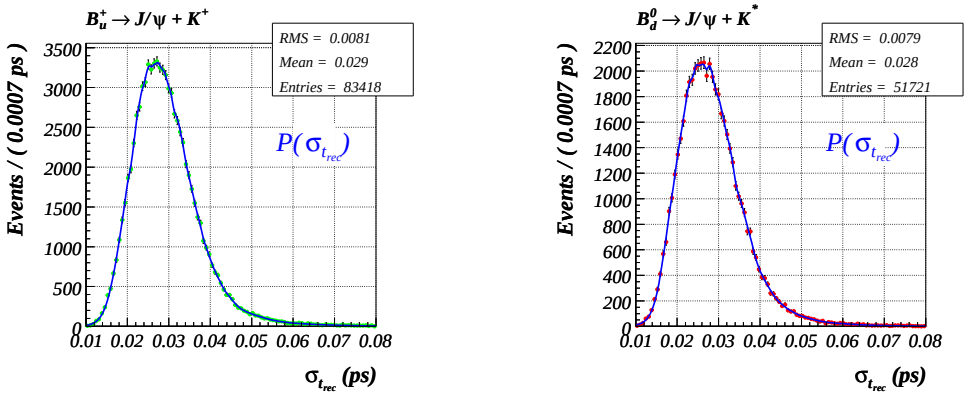

Figure 8: *The $\sigma_{t_{rec}}$ distributions for both channels, as in Fig. 7, but now with superimposed RooKeysPdf's.*

4.4 Determination of the Resolution Model Parameters

The method we used for extracting the resolution model parameters is characterized by the following points:

◇ 1.) The per-event-error distribution [$\sigma_{t_{rec}}$], Fig. 7, is sliced into N bins. The bin interval is chosen such that an equal amount of entries fall inside each bin. For each slice k the average $\langle\sigma_{t_{rec}}(k)\rangle$ is calculated.

◇ 2.) For each $\sigma^i_{t_{rec}} \in$ given bin k, the residual $x^i = t^i_{rec} - t^i_{true}$ is calculated, plotted and fitted with the function $R(x;\vec{p})$, Eq. (7). From the fits we get back $5 \times N$ different parameters, describing the residual distribution in each $\sigma_{t_{rec}}$ slice, as is shown in Fig. 9.

◇ 3.) The N sets of parameters $\vec{p_k}$, extracted from the local slice fit are expressed as a function of $\langle\sigma_{t_{rec}}(k)\rangle$, $\vec{p} = \vec{p}(\langle\sigma_{t_{rec}}(k)\rangle)$ and fitted in their turn appropriately, Fig. 10. The fitting functions are chosen to be $f(x) = p_0$ and $f(x) = p_0 + p_1 x$ [4]:

$$M(\langle\sigma_{t_{rec}}\rangle) = p_1^M \langle\sigma_{t_{rec}}\rangle \ , \tag{9}$$

$$S(\langle\sigma_{t_{rec}}\rangle) = p_1^S \langle\sigma_{t_{rec}}\rangle \ , \tag{10}$$

$$f_1(\langle\sigma_{t_{rec}}\rangle) = p_0^{f_1} \ , \tag{11}$$

$$f_2(\langle\sigma_{t_{rec}}\rangle) = p_0^{f_2} \ , \tag{12}$$

$$\tau(\langle\sigma_{t_{rec}}\rangle) = p_1^\tau \langle\sigma_{t_{rec}}\rangle \ . \tag{13}$$

At the end of this step the parameters $p_1^M, p_1^S, p_0^{f_1}, p_0^{f_2}, p_1^\tau$ are determined. (For example, we observe, as expected, that the Gaussian width S increases linearly with increasing $\langle\sigma_{t_{rec}}\rangle$.)

◇ 4.) Since $\vec{p}$ depends on $\sigma_{t_{rec}}$ (more precisely on $\langle\sigma_{t_{rec}}\rangle$), Eq. (7) can be rewritten as:

$$\begin{aligned} R(x) = \frac{N}{\sqrt{2\pi}} \Bigg[& (1 - f_1(\sigma_{t_{rec}}) - f_2(\sigma_{t_{rec}})) e^{-\frac{1}{2}\left(\frac{x - M(\sigma_{t_{rec}})}{S(\sigma_{t_{rec}})}\right)^2} \\ & + f_2(\sigma_{t_{rec}}) e^{-\frac{1}{2}\left(\frac{x}{S_{fixed}}\right)^2} \\ & + f_1(\sigma_{t_{rec}}) \left(e^{-\frac{1}{2}\left(\frac{x}{S(\sigma_{t_{rec}})}\right)^2} \otimes e^{-\left(\frac{x}{\tau(\sigma_{t_{rec}})}\right)} \right) \Bigg] \ . \end{aligned} \tag{14}$$

Plugging in the relations from Eq. (10) - Eq. (9), we see that $R(x)$ depends only on $p_1^M, p_1^S, p_0^{f_1}, p_0^{f_2}, p_1^\tau$ [5], which were determined in the previous step. That means that now we have a resolution model with a limited number of parameters.

[4] f_1 and f_2 were fitted with a function $f(x) = p_0$, while M, S and τ, with $f(x) = p_0 + p_1 x$. In the latter case, the parameter p_0 was neglected in the subsequent analysis, since it was found to be close to 0.

[5] Further on, we use the notation: $p_1^M \equiv GM$, $p_1^S \equiv GS$, $p_0^{f_1} \equiv F1$, $p_0^{f_2} \equiv F2$, $p_1^\tau \equiv TAU$.

◇ 5.) Now that the dependence on $\sigma_{t_{rec}}$ chosen and included into the model, the remaining few parameters can be determined in one single, two-dimensional, unbinned maximum likelihood fit to:

$$(t^1_{rec} - t^1_{true}, \sigma_{t^1_{rec}}), (t^2_{rec} - t^2_{true}, \sigma_{t^2_{rec}}), \ldots\ldots, (t^N_{rec} - t^N_{true}, \sigma_{t^N_{rec}}) \ , \quad (15)$$

where the suffix $1, 2, \ldots N$ represents the *i*-th event, by maximizing:

$$\log\mathcal{L} = \sum_{i=1}^{N} \log R(t^i_{rec} - t^i_{true}, \sigma_{t^i_{rec}} \mid GM, GS, F1, F2, TAU) \ . \quad (16)$$

The parameters thus extracted are compared to the ones defined from the variation of the parameters determined on the various slices in the next section.

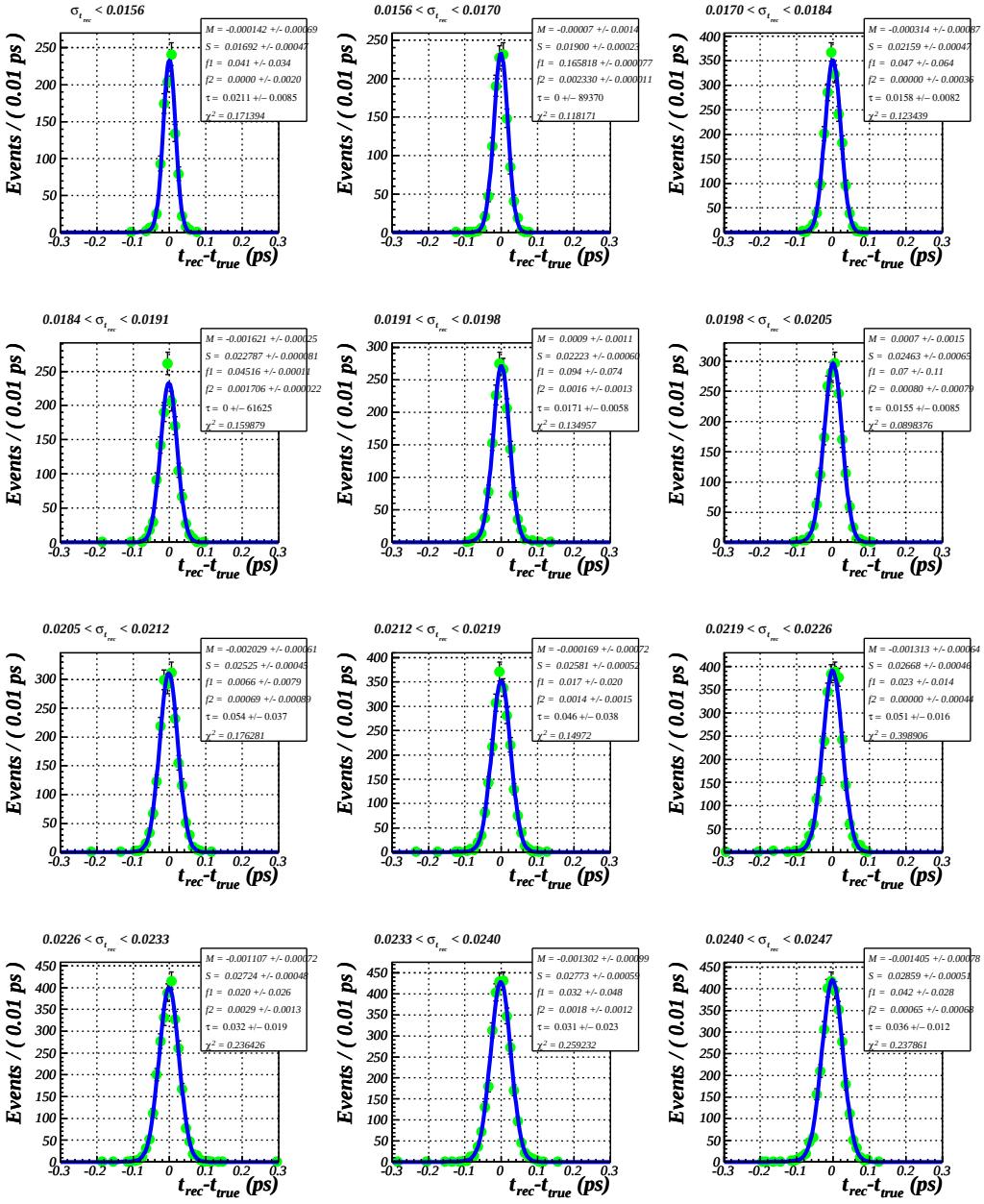

Figure 9: *The $R(x)$-fitted residual distributions for different slices of $\sigma_{t_{rec}}$. For each slice a different set of parameters is produced, using Eq. (7), i.e. without using $\sigma_{t_{rec}}$ dependence of the fit parameters. The decay channel is $B^+ \to J/\psi K^+$.*

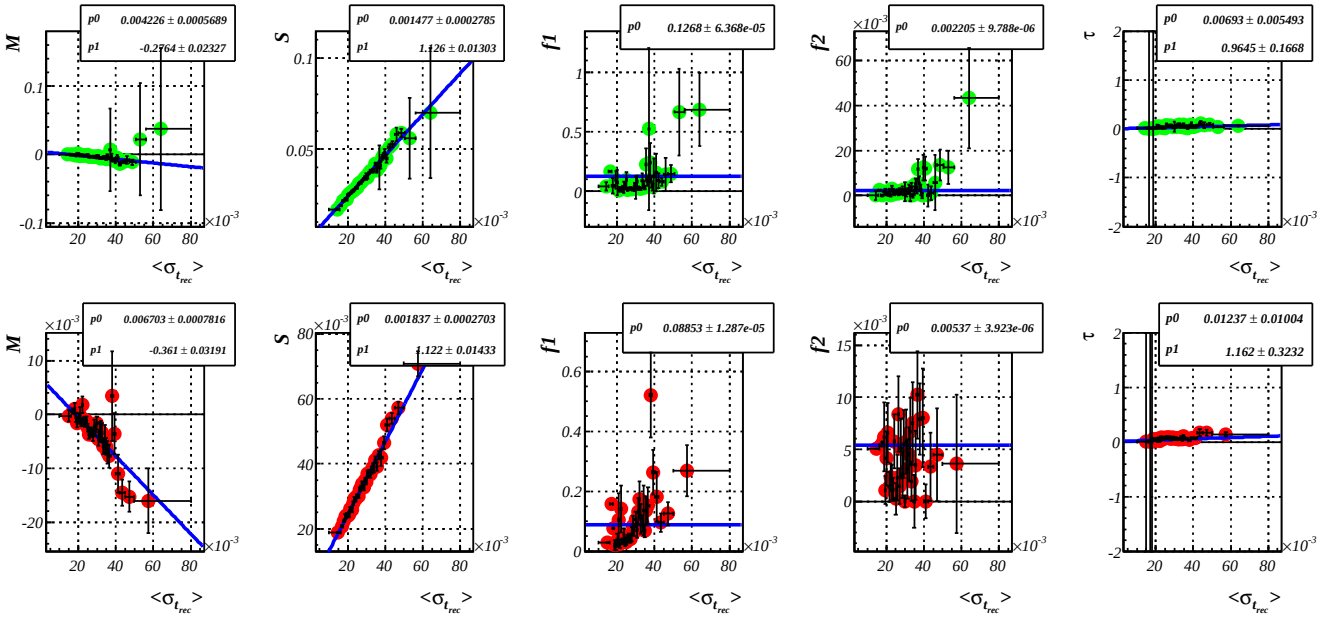

Figure 10: *The extracted $R(x)$ parameters as a function of $\langle\sigma_{t_{rec}}\rangle$. Up: $B^+ \to J/\psi K^+$, Down: $B^0 \to J/\psi K^*$.*

4.5 Validation of the model

As previously discussed in Sec. 4.4, to validate the so built resolution model, an unbinned maximum likelihood fit to the data points - Eq. (15) is done. Plots in 2D and 3D revealing the $(t^i_{rec} - t^i_{true})$ vs. $\sigma_{t^i_{rec}}$ dependency are displayed in Fig. 11. The projection of the fit on the $(t_{rec} - t_{true})$ axis can be expressed with:

$$\mathcal{R}(t_{rec} - t_{true})_{proj} = \int_0^\infty d\sigma_{t_{rec}} R(t_{rec} - t_{true} \mid \sigma_{t_{rec}}) \times P(\sigma_{t_{rec}}) \ . \qquad (17)$$

The results from the unbinned, *global* fit are presented in Fig. 12 and Fig. 13, where the fit projections on the $(t_{rec} - t_{true})$ axis are shown by the curve. The extracted values of the fit parameters are displayed in the statistics box. Note that the fractions $F1$ and $F2$ are relatively small, indicating that the resolution is mainly determined by the first term in Eq. (14), i.e. the simple Gaussian.
To see whether the unbinned fit correctly describes the time residual distributions in the various ranges of $\sigma_{t_{rec}}$, we have also projected $\mathcal{R}(x)$ in individual slices of $\sigma_{t_{rec}}$ and have examined the quality of the fit. These projections of the global fit on the residual distribution are shown in Fig. 14 for the different $\sigma_{t_{rec}}$ ranges, for the channel $B^+ \to J/\psi K^+$. Remark that the fit parameters are the same for all the slices, since the curves shown are projections over different intervals of $\sigma_{t_{rec}}$ of the same global likelihood[6].
The plots in Fig. 15 and Fig. 16 illustrate the residuals and the pulls for the fits given in Fig. 14. The values of the pulls are nicely spread around zero, Fig 17.

[6]Note that the curves *do* depend on the selected slice, as the projections differ because the interval over which $\sigma_{t_{rec}}$ is integrated in Eq. 17 varies. This is one of the reasons we have explicitly included the conditional pdf for $\sigma_{t_{rec}}$ in our likelihood

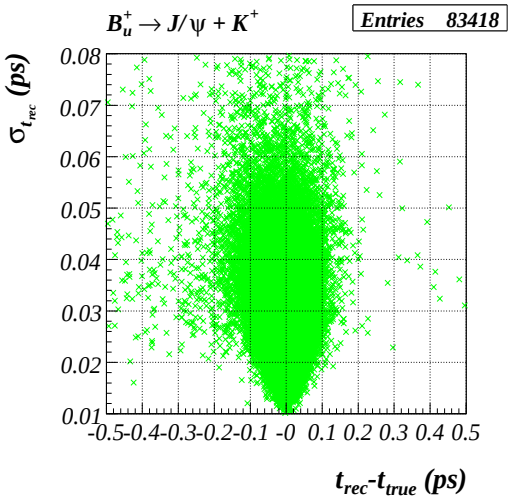

(a) *2D plot of* $[t_{rec} - t_{true}]$ *vs.* $[\sigma_{t_{rec}}]$ *for* $B^+ \to J/\psi K^+$.

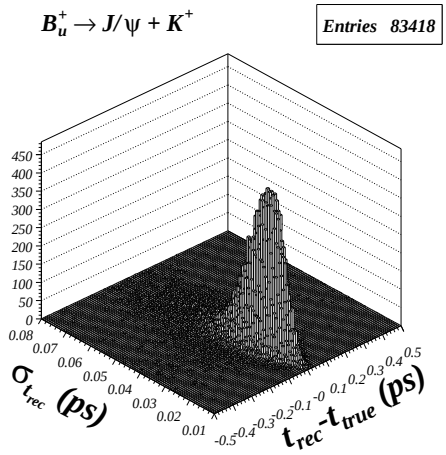

(b) *3D plot of* $[t_{rec} - t_{true}]$ *vs.* $[\sigma_{t_{rec}}]$ *for* $B^+ \to J/\psi K^+$.

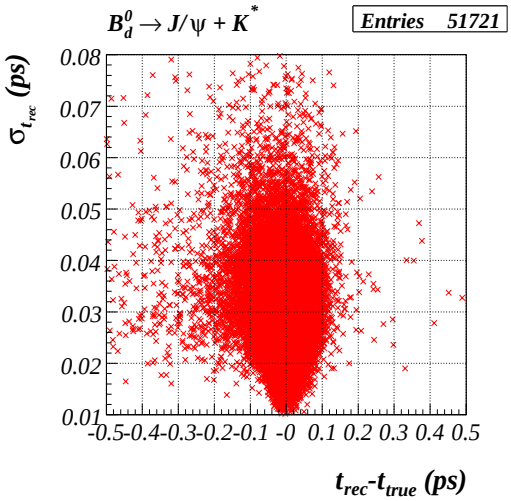

(c) *2D plot of* $[t_{rec} - t_{true}]$ *vs.* $[\sigma_{t_{rec}}]$ *for* $B^0 \to J/\psi K^*$

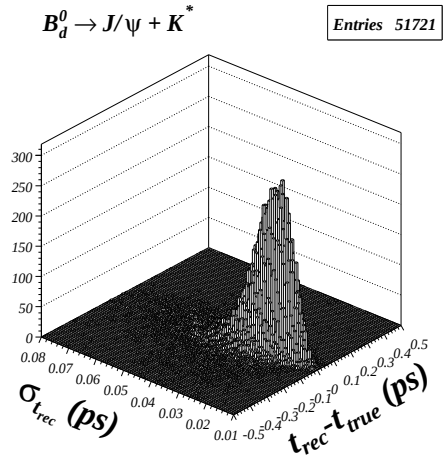

(d) *3D plot of* $[t_{rec} - t_{true}]$ *vs.* $[\sigma_{t_{rec}}]$ *for* $B^0 \to J/\psi K^*$

Figure 11: *2D and 3D plots of* $[t_{rec} - t_{true}]$ *vs.* $[\sigma_{t_{rec}}]$ *for both channels.*

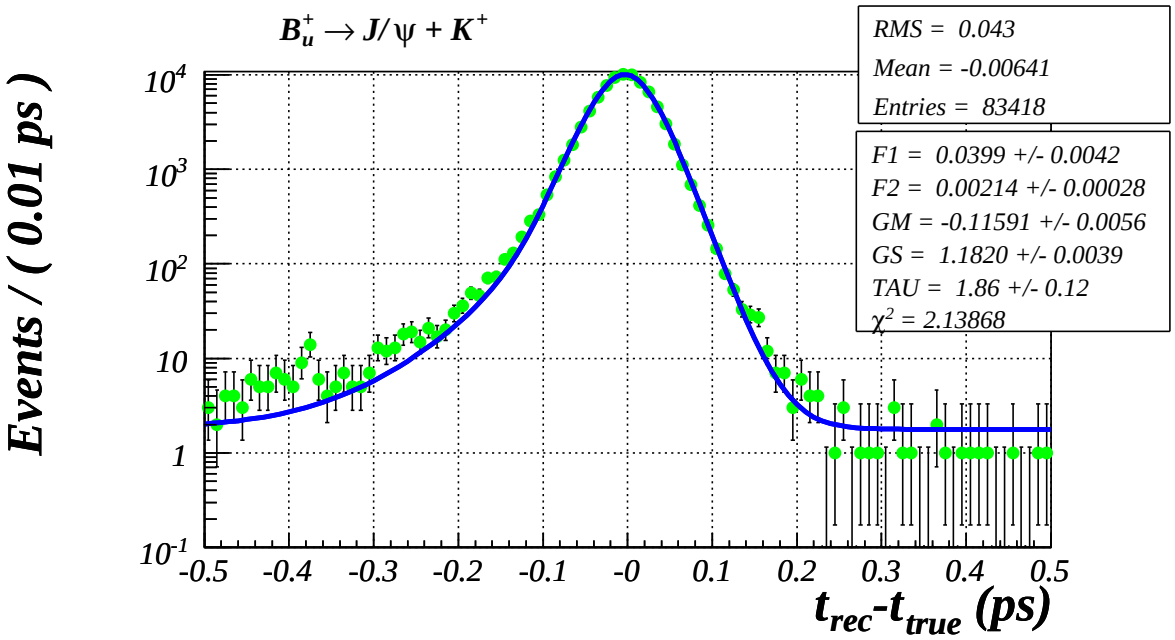

Figure 12: *Projections of the global, unbinned fit onto* $[t_{rec} - t_{true}]$ *axis for channel* $B^+ \to J/\psi K^+$

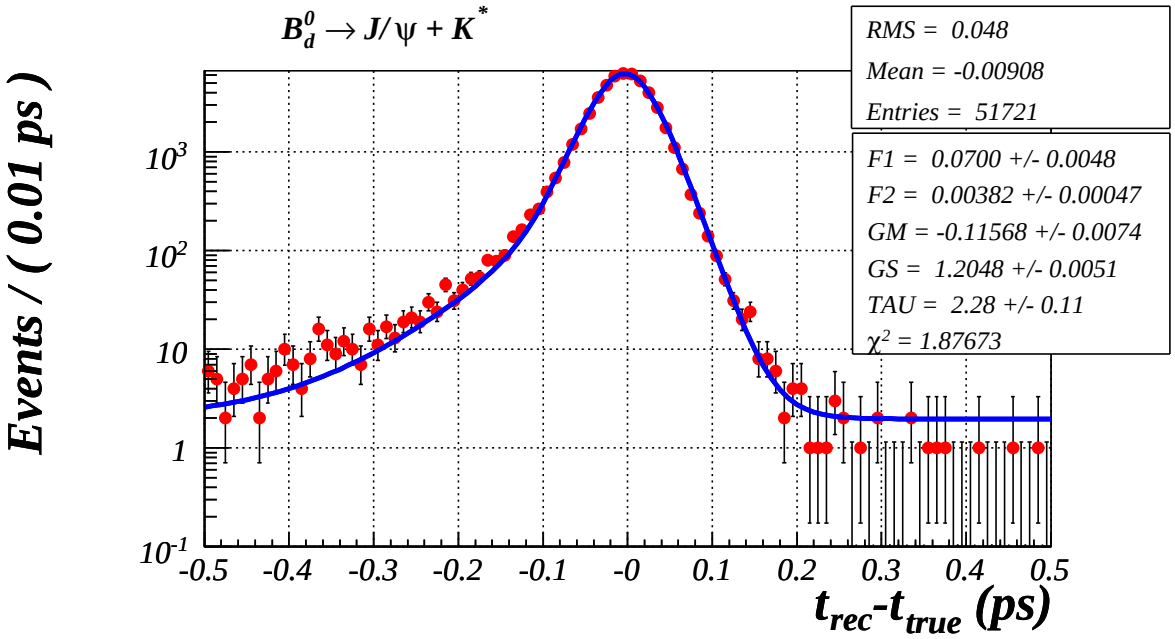

Figure 13: *Projections of the global, unbinned fit onto* $[t_{rec} - t_{true}]$ *axis for channel* $B^0 \to J/\psi K^*$.

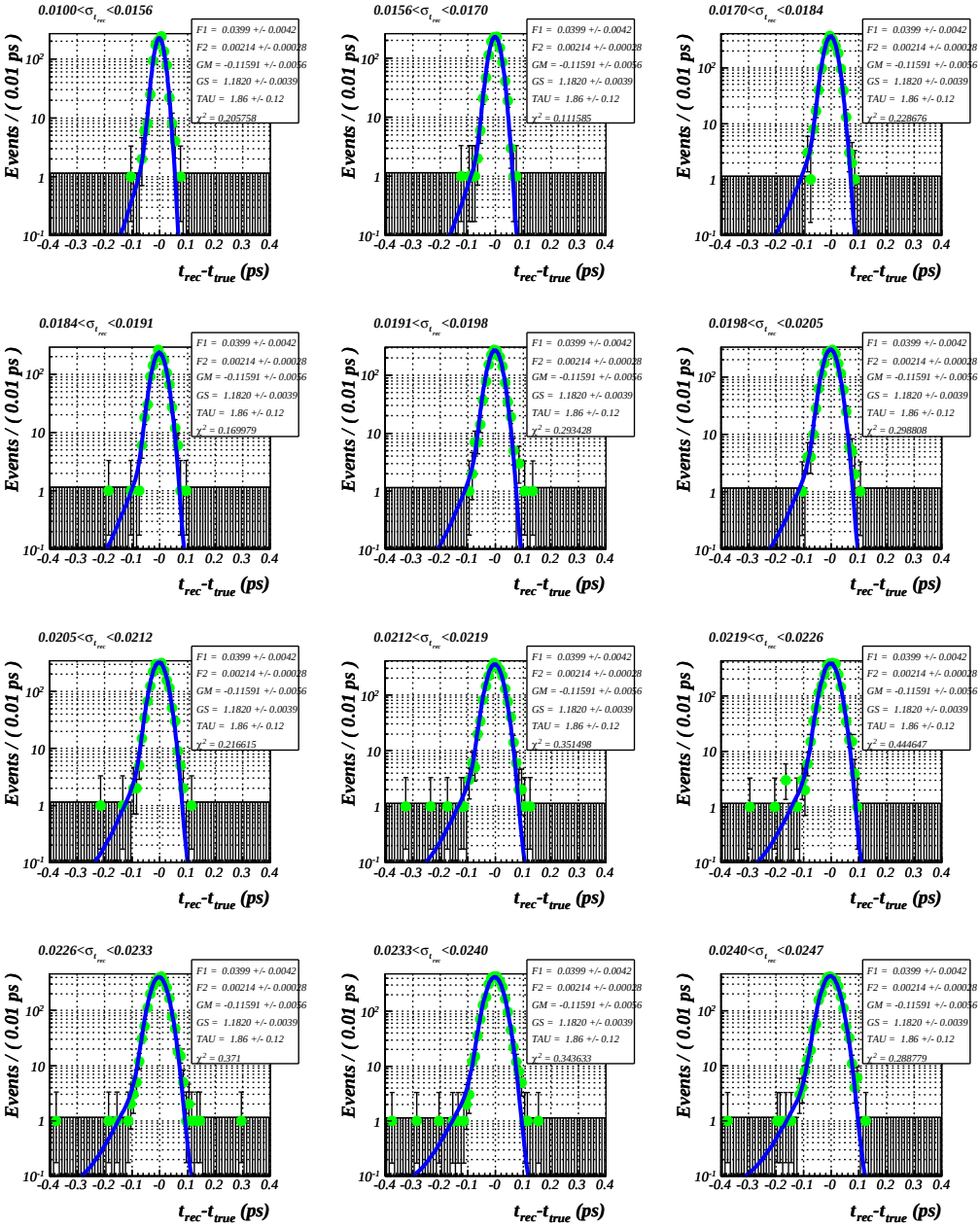

Figure 14: *Projections of the global unbinned maximum likelihood fit, using Eq. (17), onto the* $[t_{rec} - t_{true}]$ *axis in intervals of* $\sigma_{t_{rec}}$ *for the channel* $B^+ \to J/\psi K^+$.

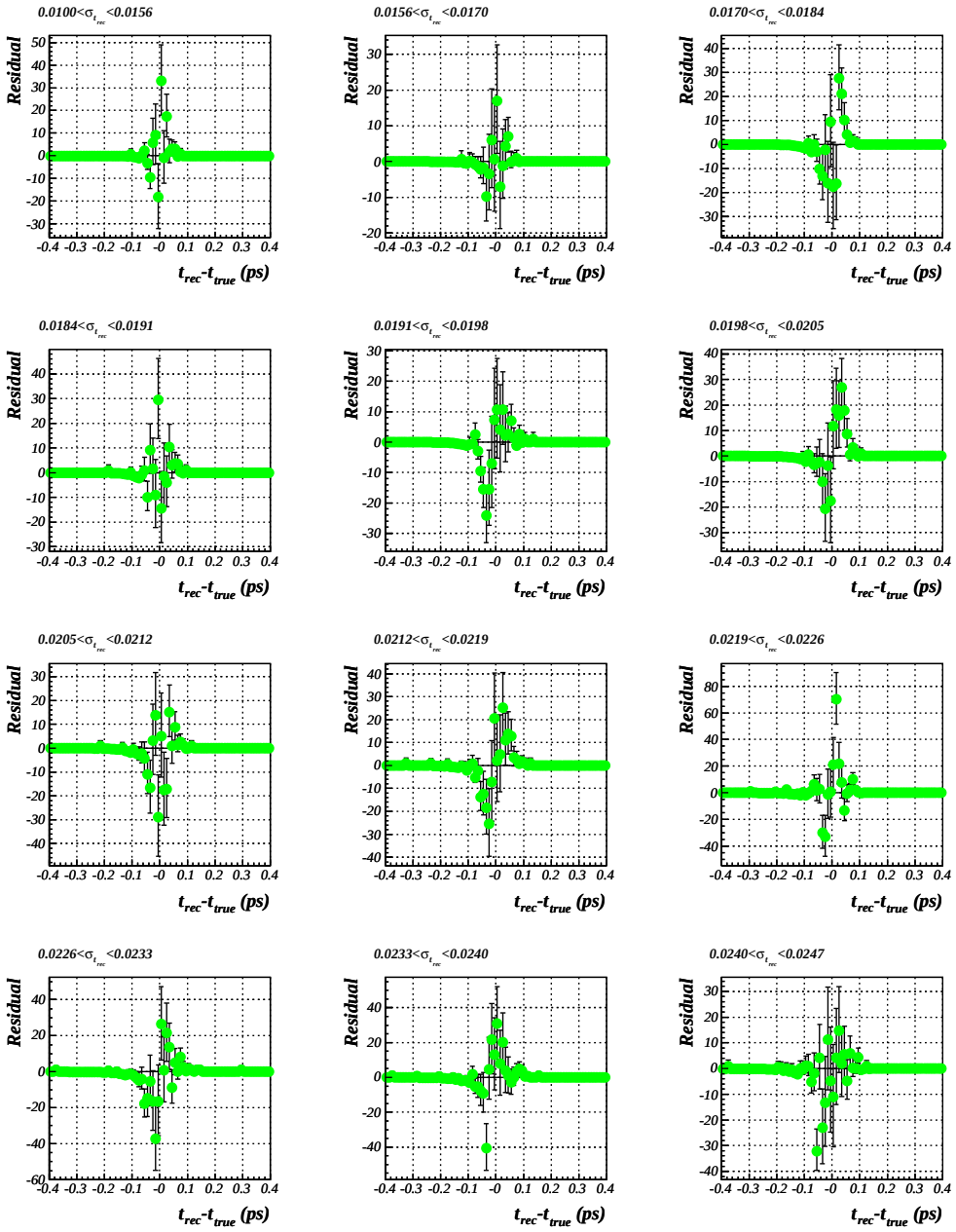

Figure 15: *Fit residuals for the various projections of the global unbinned maximum likelihood fit onto* $[t_{rec} - t_{true}]$ *axis in different intervals of* $\sigma_{t_{rec}}$ *for the channel* $B^+ \to J/\psi K^+$.

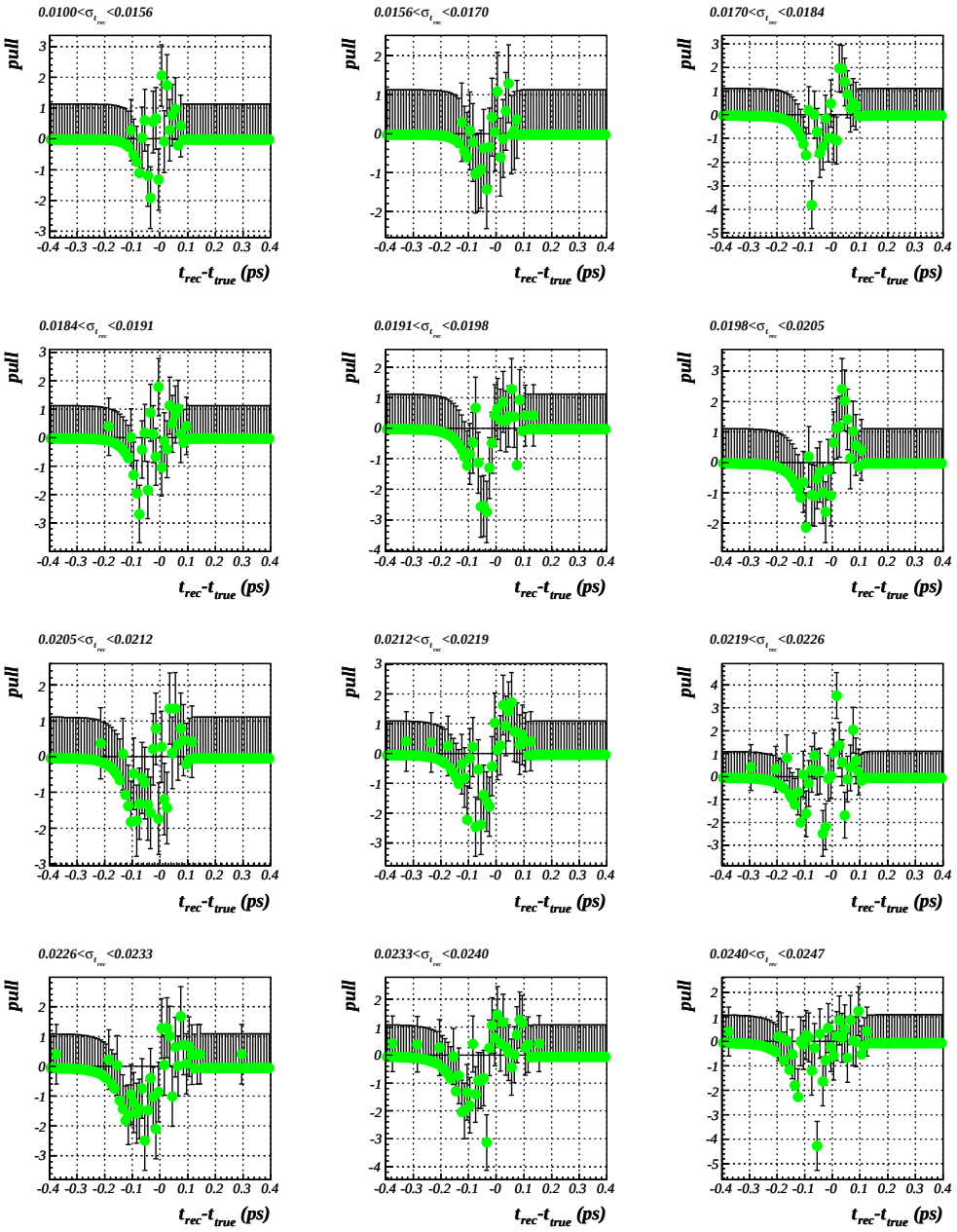

Figure 16: *Pulls for the various projections of the global unbinned maximum likelihood fit onto* $[t_{rec} - t_{true}]$ *axis in different intervals of* $\sigma_{t_{rec}}$ *for the channel* $B^+ \to J/\psi K^+$.

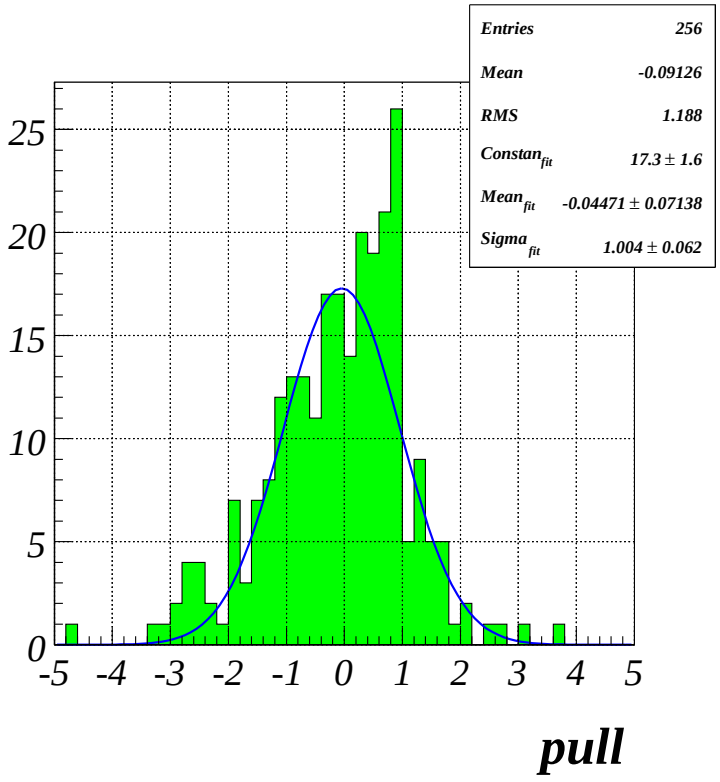

Figure 17: *Distribution of the pulls for the projection of the global unbinned maximum likelihood fit onto* $[t_{rec} - t_{true}]$ *axis for* $B^+ \rightarrow J/\psi K^+$*. Only the pulls for bins that contain more than 3 entries (Fig. 12) are plotted. The histogram is fitted with a Gaussian function.*

5 Determination of the parameters on real data

5.1 Method

At this point, we have obtained a resolution model with 5 parameters that attempts to describes the decay time residuals $t^i_{rec} - t^i_{true}$ for all values of $\sigma_{t_{rec}}$.
In reality, we will not have access to t_{true}. The only two available observables are t_{rec} and its uncertainty $\sigma_{t_{rec}}$. Here, we shall try to determine the resolution model parameters using only these two observables. To do this, we must build an appropriate p.d.f. describing the t_{rec} distribution. We know that for an ideal detector the distribution of the observed decay times t_{true} is a falling exponential distribution of the type:

$$E(t) = e^{-\frac{t}{\tau}} \ , \tag{18}$$

where τ is the mean lifetime of the B meson. Then, the reconstructed proper-time's p.d.f $F(t_{rec}, \sigma_{t_{rec}})$ is a falling exponent too, but smeared with the detector resolution. We can write $F(t_{rec}, \sigma_{t_{rec}})$ as a convolution between $E(t_{rec})$ and $\mathcal{R}(t_{rec} \mid \sigma_{t_{rec}})$:

$$F(t_{rec}, \sigma_{t_{rec}}) = E(t_{rec}) \otimes \mathcal{R}(t_{rec} \mid \sigma_{t_{rec}}) = \left[\int dt' e^{-\frac{t'}{\tau}} R(t - t' \mid \sigma_{t_{rec}}) \right] \times P(\sigma_{t_{rec}}) \ . \tag{19}$$

By performing an unbinned maximum likelihood fit with this p.d.f. to the observed $[t^i_{rec}, \sigma^i_{t_{rec}}]$ pairs, we are able to determine the resolution model parameters. Note that now, we have six fit parameters - the five ones from the resolution model plus the B lifetime τ_B, which is a free parameter and will be extracted from the global fit. Take into consideration that most information on the decay time resolution is obtained from the events with $t_{rec} \approx 0$, since in this region the distortion of the sharp rising edge of the exponential at $t = 0$ by the resolution is most pronounced. As a result it is important to test whether the resolution obtained from these events is representative of the entire sample, i.e. whether the resolution does *not* depend on the proper-time itself.
In the next subsection we will compare the resolution model parameters retrieved using $t_{rec} - t_{true}$, to the ones obtained using only t_{rec}.

5.2 Results

Figures 18 and 19 show the projection of the unbinned fit to the t_{rec} axis for both investigated decay modes. The corresponding fit residual and pull distributions are also given, indicating the quality of the fit.
The extracted resolution model parameters through a global fit (Eq. (19)) to the reconstructed simulation data are given in Table 3 (for $B^+ \to J/\psi K^+$) and Table 4 (for $B^0 \to J/\psi K^*$) together with the parameter values obtained from the global fit to the time residuals using t_{true}.
Comparing the two sets of values we come to the following conclusions:

- The mean lifetimes $\tau_{B^{+/0}}$ of the B^+ and B^0 respectively, are determined to a precision of 6 fs. The τ_B values match remarkably well with the ones received from the fit to t_{true} (the fit outputs in Table 2).

- The fraction parameter $F1$, the fraction that allows for a modified decay time distribution, differs by a factor 0.1 and 4 for $B^+ \to J/\psi K^+$ and $B^0 \to J/\psi K^*$, respectively.

- The scale factor for the bias, GM, for both channels, indicates that a larger bias in the decay time is observed in the data.

* A smaller resolution scale factor GS, is seen in the data for both channels, compared to what is expected from Monte-Carlo simulation truth.

* The values of TAU are not determined accurately from the data, which in the case of $B^+ \to J/\psi K^+$ can be attributed to the very small fraction $F1$.

Parameter	Fit to $(t_{rec} - t_{true})$	Error	Fit to t_{rec}	Error	Global Correlation
τ_{B^+}			1.6997	0.0057	0.1791
F1	0.0399	0.0042	0.0034	0.0009	0.8333
F2	0.0021	0.0003	0.0005	0.0003	0.6963
GM	-0.1159	0.0056	-0.4422	0.0289	0.4797
GS	1.1820	0.0039	0.8807	0.0280	0.5308
TAU	1.8561	0.1170	16.9820	4.7000	0.8849

Table 3: *Resolution model parameters - results. Channel:* $B^+ \to J/\psi K^+$

Parameter	Fit to $(t_{rec} - t_{true})$	Error	Fit to t_{rec}	Error	Global Correlation
τ_{B^0}			1.5233	0.0065	0.1581
F1	0.0700	0.0048	0.2808	0.1480	0.9858
F2	0.0038	0.0005	0.0014	0.0003	0.1918
GM	-0.1157	0.0074	-0.4935	0.0559	0.7554
GS	1.2048	0.0051	0.4594	0.0761	0.8902
TAU	2.2831	0.1110	1.1098	0.2230	0.9759

Table 4: *Resolution model parameters - results. Channel:* $B^0 \to J/\psi K^*$

Note that the difference between the decay channels can be explained by the fact that $F1$ and GS are correlated, given that a larger fraction $F1$ can be compensated by a smaller width GS.

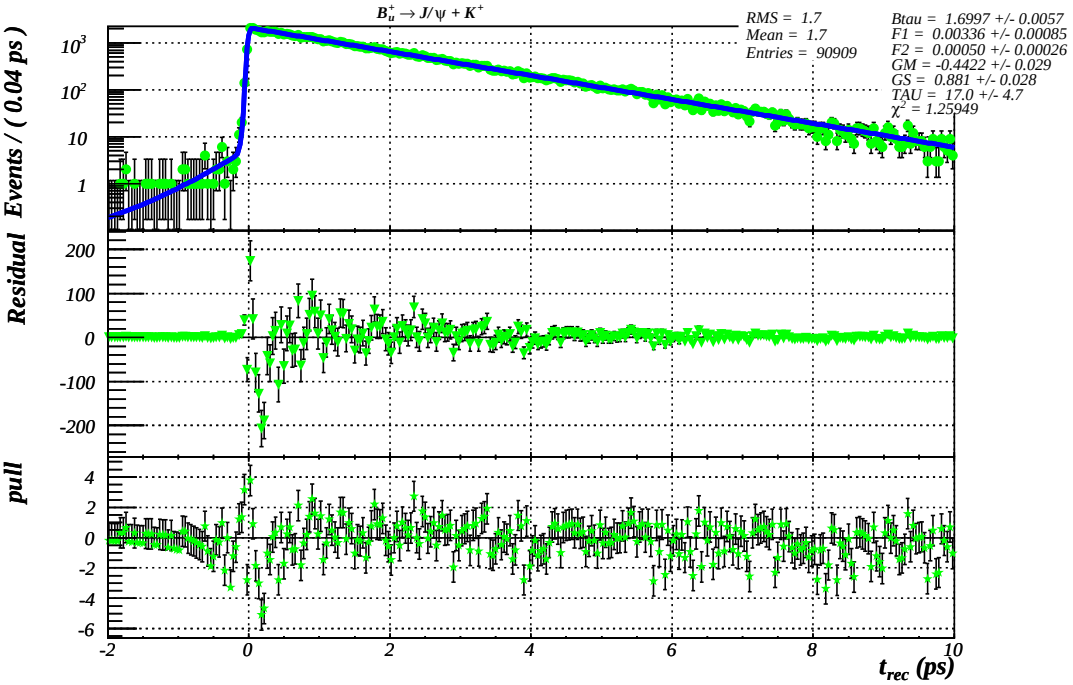

Figure 18: *Projection of the global-unbinned fit to t_{rec} for channel $B^+ \to J/\psi(1S)K^+$. Fit residuals and pulls are given also.*

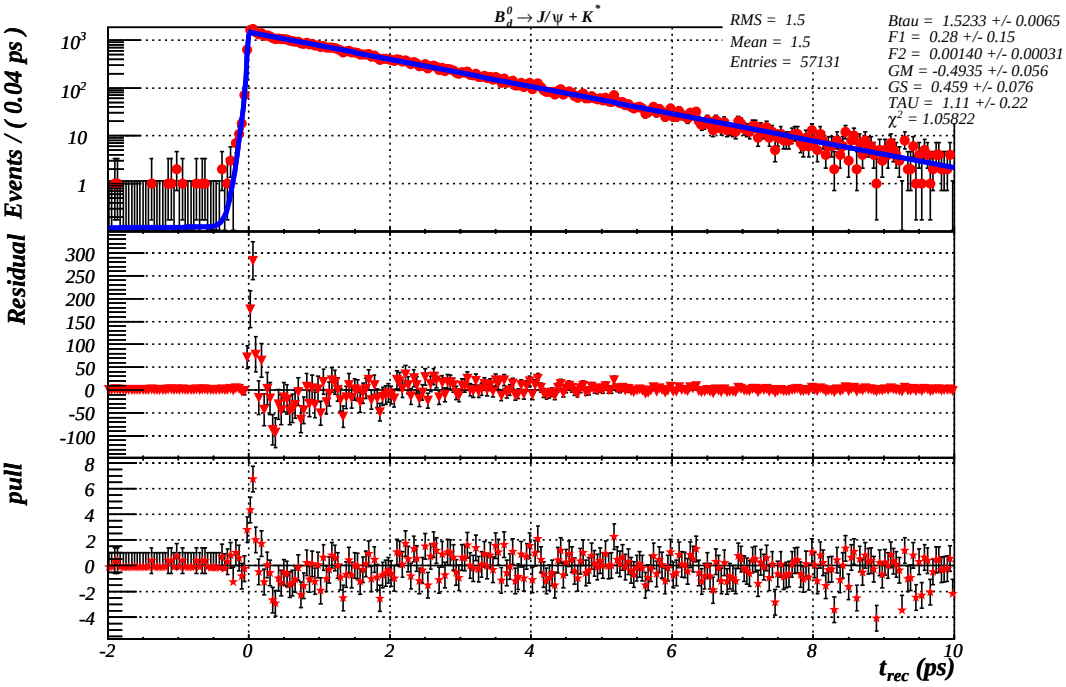

Figure 19: *Projection of the global-unbinned fit to t_{rec} for channel $B^* \to J/\psi(1S)K^*$. Fit residuals and pulls are given also.*

6 Dependence on t_{true}

6.1 Test for dependence on t_{true}

By construction, the resolution model does not depend explicitly on the true proper-time t_{true} of the B meson. It does depend on the difference $(t_{rec} - t_{true})$ but not on t_{true}. Any dependence on t_{true} is a sign of a bias.
To see whether there is a correlation between the true proper-time and the proper-time resolution, we sliced the t_{true} distributions, Fig. 20, into bins and applied the resolution model (see Section 4) to the decay time residuals $(t_{rec} - t_{true})$ falling into each bin of t_{true}.

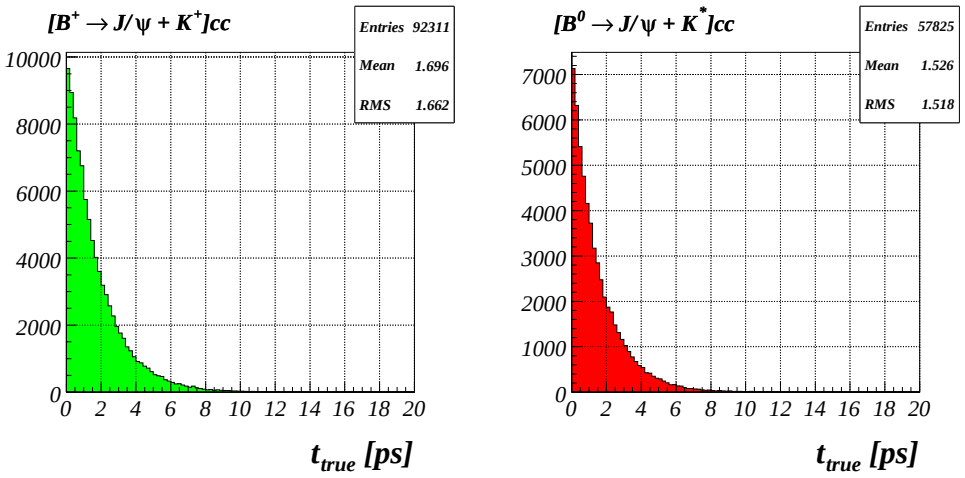

Figure 20: t_{true} *distributions for both channels.*

The t_{true} slicing is done as follows:

- The true proper-time distribution t_{true}, Fig. 20, is sliced into N bins. The bin interval is chosen such that an equal amount of entries falls in each bin.
- For each $t^i_{true} \in$ given bin k, the residual $x^i = t^i_{rec} - t^i_{true}$ is calculated, plotted and fitted with the function $R(x;\vec{p})$, Eq. (7).

In Fig. 21 and Fig. 22 the residual distributions are presented in slices of t_{true} fitted with $R(x)$ (Eq. (7)) in each slice separately, for both studied channels.
Following the procedure as described in Section 4.4, subsequently we include the per-event-error in the fit and perform an unbinned maximum likelihood fit for each t_{true} slice.

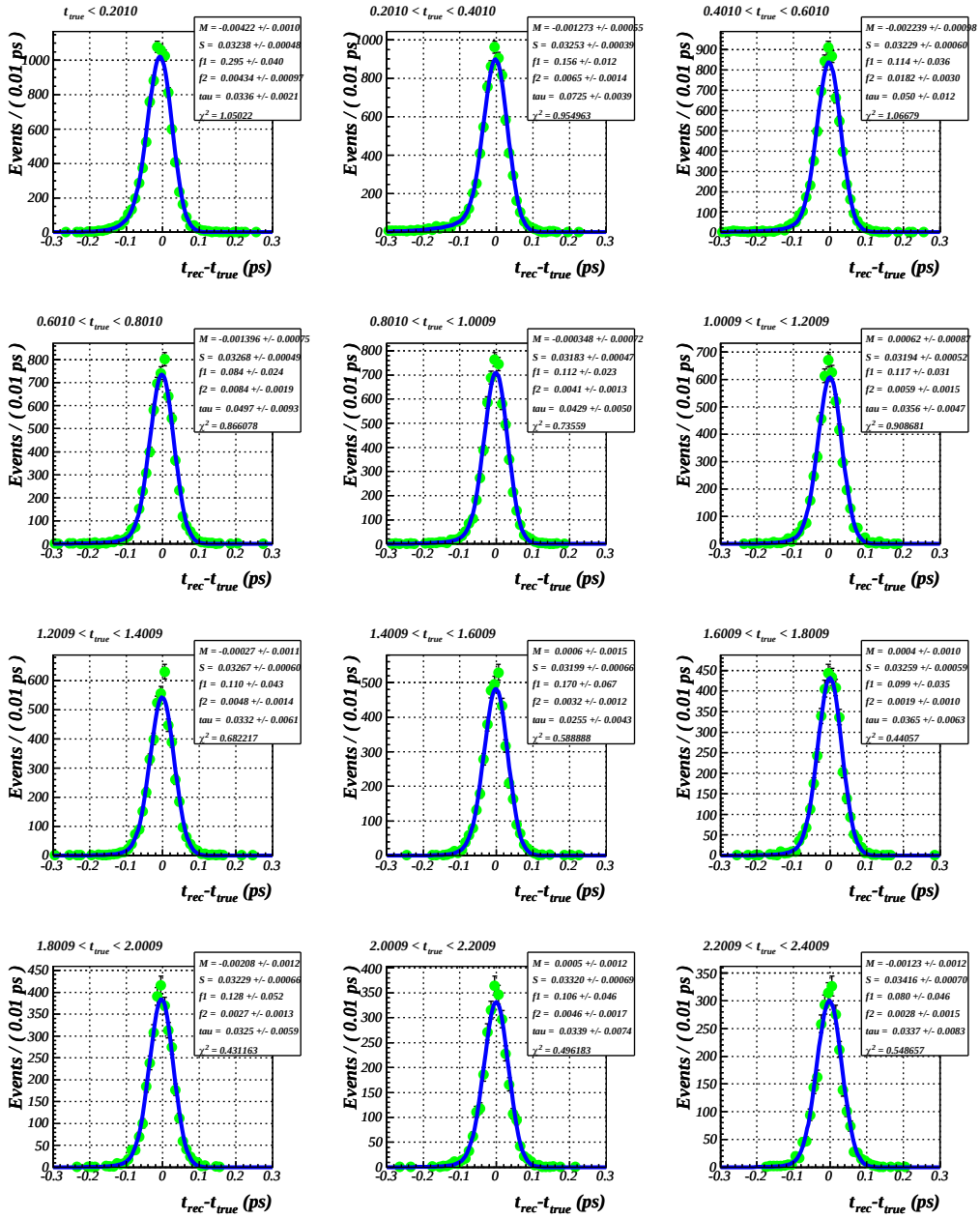

Figure 21: *The $R(x)$-fitted residual distributions for different slices of t_{true}, using Eq.(7). The decay channel is $B^+ \to J/\psi K^+$.*

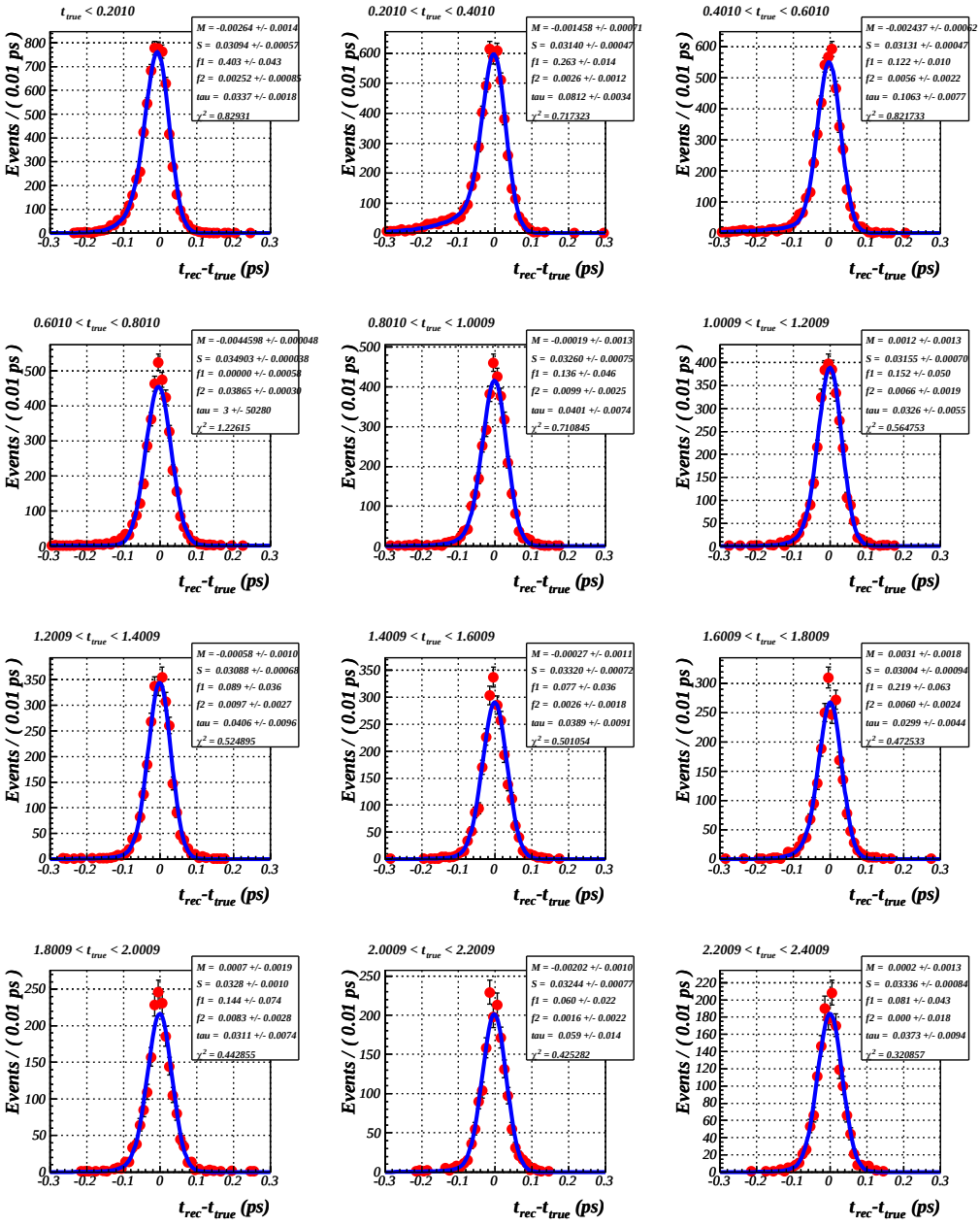

Figure 22: *The $R(x)$-fitted residual distributions for different slices of t_{true}, using Eq.(7). The decay channel is $B^0 \to J/\psi K^*$.*

For each t_{true} interval, the $\sigma_{t_{rec}}$ errors are plotted with their p.d.f.'s, obtained via the ROOKEYSPDF method [7], as shown in Fig. 24.
The decay time residuals can be fitted with the unbinned maximum likelihood fit (Eq.(16)) separately, in each given t_{true} bin. The projections of that fit (Eq. (17)) onto the $(t_{rec} - t_{true})$ axis for the slices of t_{true} for both channels is shown in Fig. 25 and Fig. 26. From these figures one can easily see that the behaviour of the residual distributions vary with the slices. The parameters of the global fit for each slice vary too. These parameters are quite different for the first several slices in comparison with the others (see *GS* and *TAU* for example). The conclusion is that we observe a clear evidence for a dependence of the resolution on the true proper-time.

6.2 Explanation of the t_{true} dependence

A possible explanation for the resolution dependence on t_{true} is the hypothesis that the reconstruction of the primary vertex (PV) is biased. The PV could be biased as some of the B decay products are used in the PV reconstruction. If this is the case, then we would have smaller reconstructed B meson travel path d_{rec}, which would lead to smaller reconstructed proper-time t_{rec} and hence to abnormally smaller decay time residual $(t_{rec}-t_{true})$. This mechanism is illustrated in Fig. 23. According to that picture the primary vertex is attracted to the secondary (decay) vertex (SV). Since the channel $B^0 \to J/\psi K^*$ has more associated tracks, the probability that one of them is used for the PV reconstruction is higher, and therefore the effect on the dependence of the resolution on t_{true} would be stronger. And indeed, e.g. GS varies between 1.15 and 1.22 for $B^+ \to J/\psi K^+$ and between 1.13 and 1.25 for $B^0 \to J/\psi K^*$. The t_{true} dependence is slightly stronger in the B^0 decay mode.

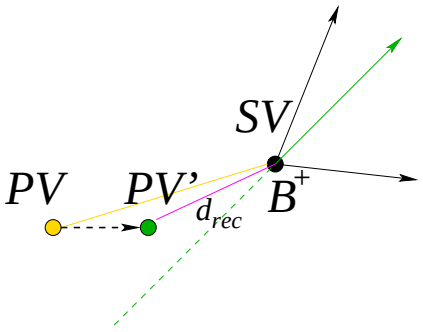

Figure 23: *Illustration of a mechanism, which could lead to a bias in the reconstruction of the primary vertex. One of the B daughters is used in the definition of the PV. There is a PV to SV "attraction".*

Again, note that the bias on the reconstructed proper-time due to other long-lived resonances is absorbed implicitly in the resolution model. As a result, as long as the bias is uncorrelated to the value of the proper-time, it is properly taken into account.

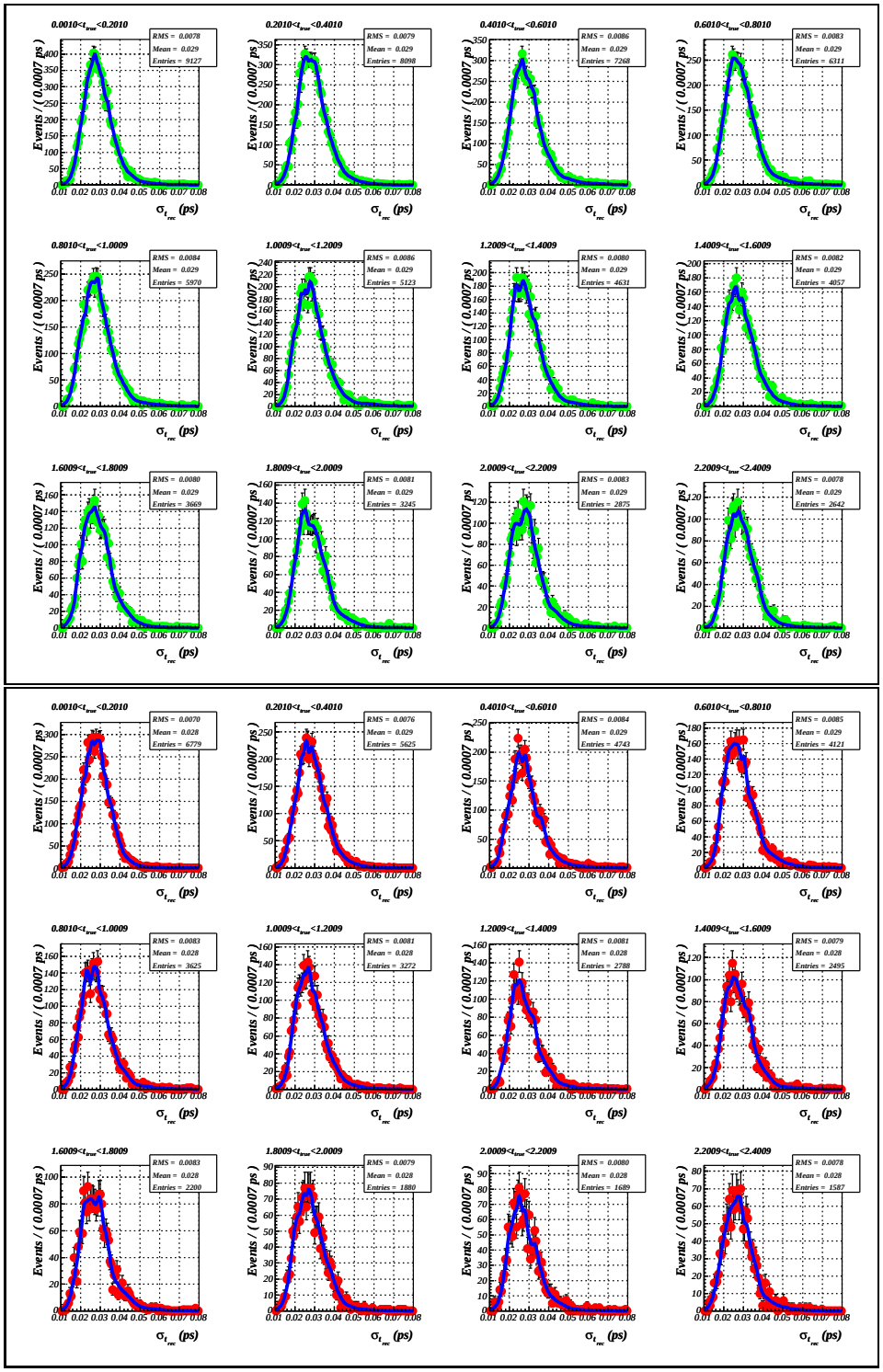

Figure 24: $\sigma_{t_{rec}}$ *distribution per* t_{true} *slice, described by RooKeysPdf. Up:* $B^+ \to J/\psi K^+$*, Down:* $B^0 \to J/\psi K^*$

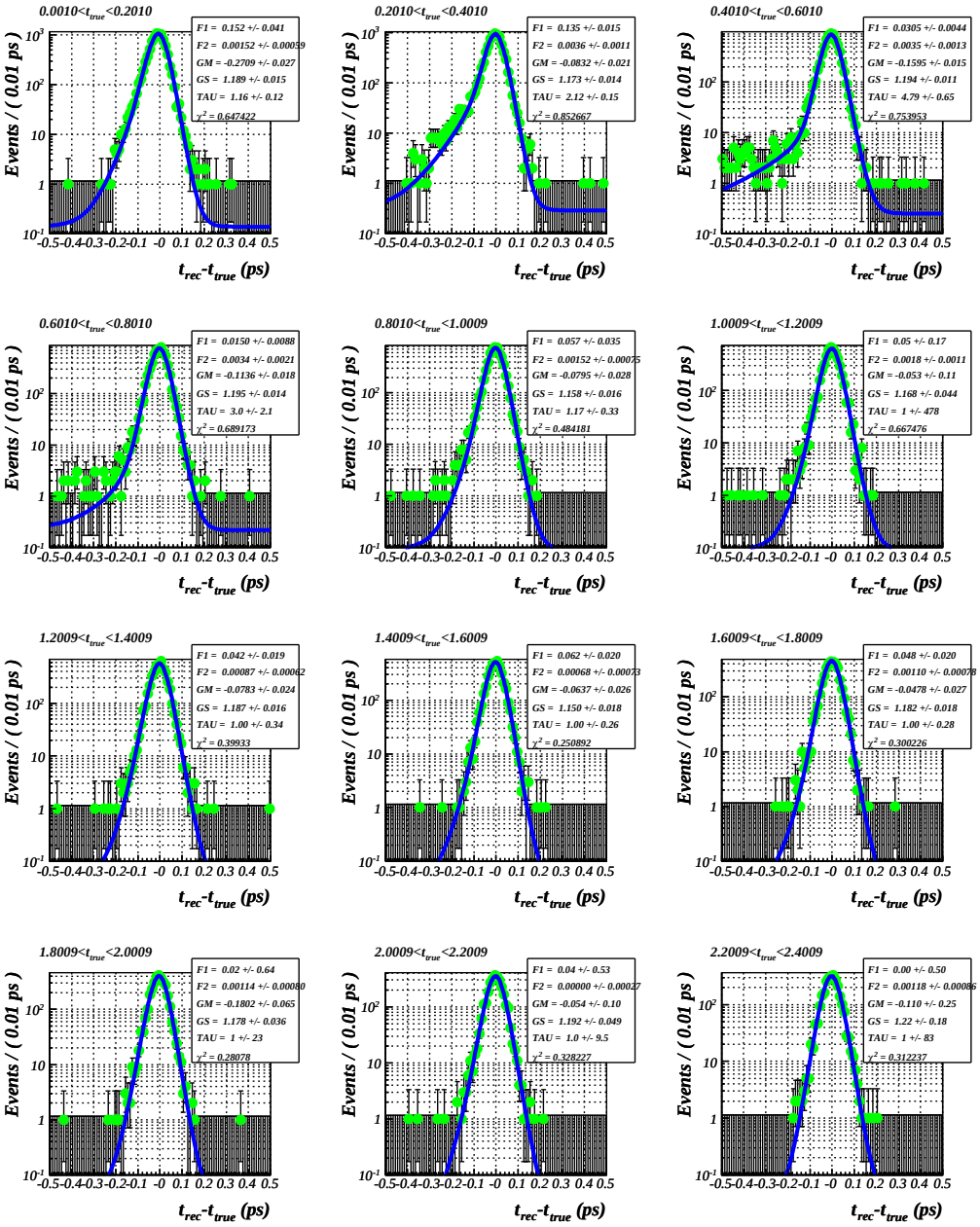

Figure 25: *Projections of the unbinned maximum likelihood fits to the* $[t_{rec} - t_{true}]$ *axis for the corresponding slices of* t_{true} *for* $B^+ \to J/\psi K^+$ *using Eq. (17).*

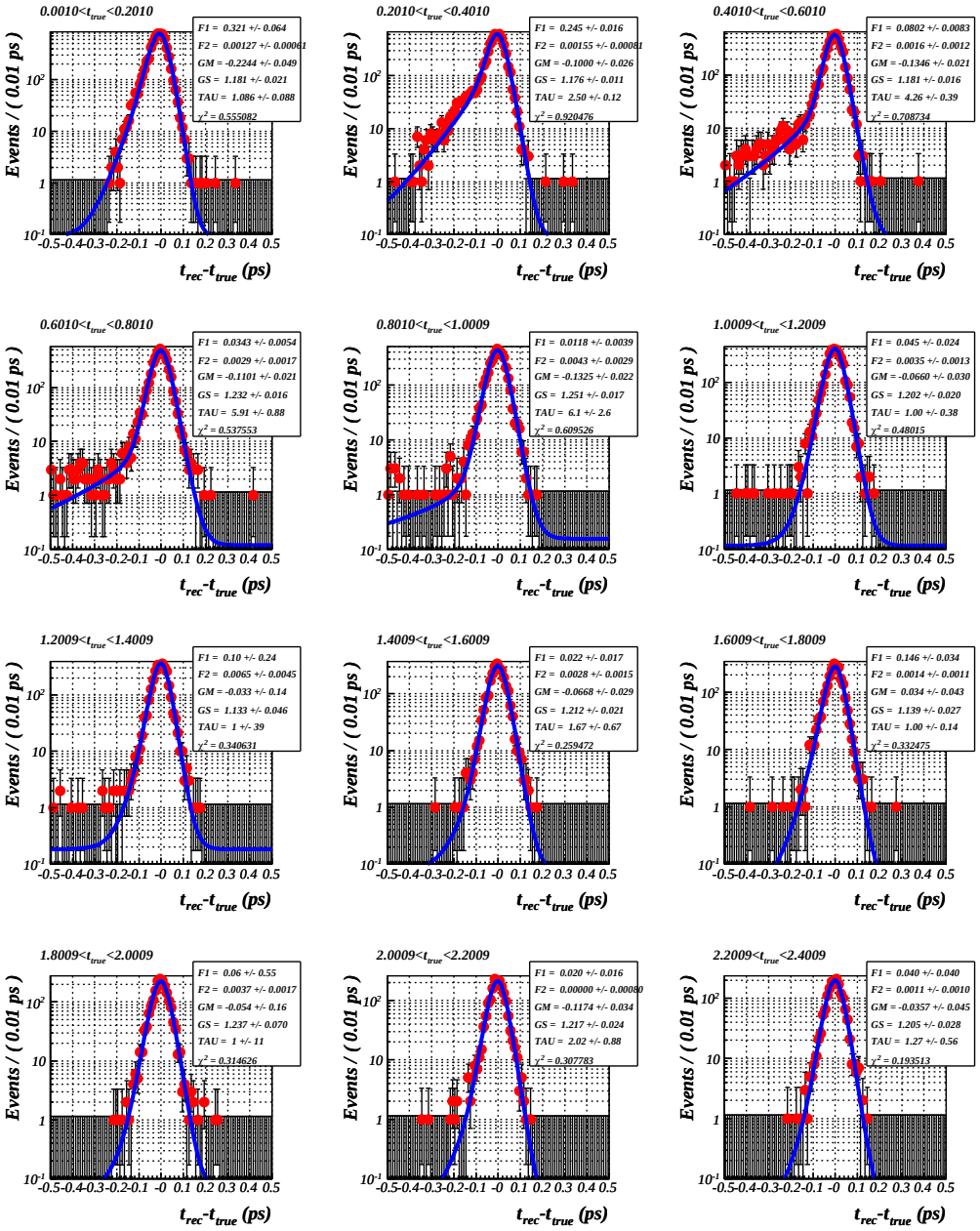

Figure 26: *Projections of the unbinned maximum likelihood fits to the* $[t_{rec} - t_{true}]$ *axis for the corresponding slices of* t_{true} *for* $B^0 \to J/\psi K^*$ *using Eq. (17).*

6.3 Primary Vertex re-definition

To check the hypothesis that the wrong reconstruction of the primary vertex is the cause for the dependence of the resolution on the true proper-time, we performed a separate study, in which we tried to re-define the PV position. The study was done with separate samples of $B^+ \to J/\psi(1S)(\mu^+\mu-)K^+$ and $B^0 \to J/\psi(1S)(\mu^+\mu-)K^*(K^+\pi^-)$ events. The selection procedure and the cuts applied were the same as those given in Section 3. The only difference is in the number of the processed evens, which is now reduced (50000 selected B^+ candidates, and 29000 selected B^0 candidates).
We re-defined the primary vertex position in the following way[7]:

- All tracks associated with the B particle are *removed* from the PV reconstruction list.
- The PV is *refitted*.

In this manner, the reconstruction of the B particle is not affected, but the PV position is updated.
We ran our event selections for the three possible cases, in order to be able to compare:

Case 1. *Original PV* - The PV is nominally reconstructed.

Case 2. *Refitted PV* - The PV is only refitted with an alternative approach.

Case 3. *Removed B's and Refitted PV* - The B associates are removed from the tracks used for PV reconstruction and then the PV is refitted and updated.

In Fig. 27 the distributions of the primary vertex coordinates X, Y and Z are shown for the three cases that we considered. The mean Z coordinate of the PV is slightly shifted from 1.271 mm to 1.263 mm, once the PV is refitted with removed B associates. The "attraction" towards the secondary vertex is reduced. This can be seen more clear in Fig. 28, where the differences in X, Y and Z are plotted for: $[PV_{orig} - PV_{refit}]$ (1st row on the graph); $[PV_{orig} - PV_{refit}]$ (2nd row) and $[PV_{rem\&refit} - PV_{refit}]$ (3rd row). The distribution of the Z differences now shows a clear shift to higher values, since Z_{orig} is bigger than $Z_{rem\&refit}$ with ~ 8 μm on average.
We will now repeat the procedure as described in Section 6.1, to verify an improved t_{true} dependence. Applying slicing in t_{true} and then fitting each slice with an unbinned maximum likelihood (Eq. (17)) we get the results presented in Fig. 29, Fig. 30 and Fig. 31 for the three cases of the PV position for $B^+ \to$

[7]The PVREFITTER DaVinci algorithm was used.

$J/\psi K^+$ channel. For $B^0 \to J/\psi K^*$ channel the analogous plots are given in Fig. 32, Fig. 33 and Fig. 34. Only the first four slices in t_{true} with the largest true proper-time dependence are shown. Comparing the figures one can see that there is an improvement, although a dependence on t_{true} is still present. Both GM and the resolution scale factor GS, improve with improved PV reconstruction.
The projection of the global-unbinned fit to t_{rec}, the fit residuals and the fit pulls for both channels, when PV is updated, can be seen in Fig. 35 and Fig. 36.

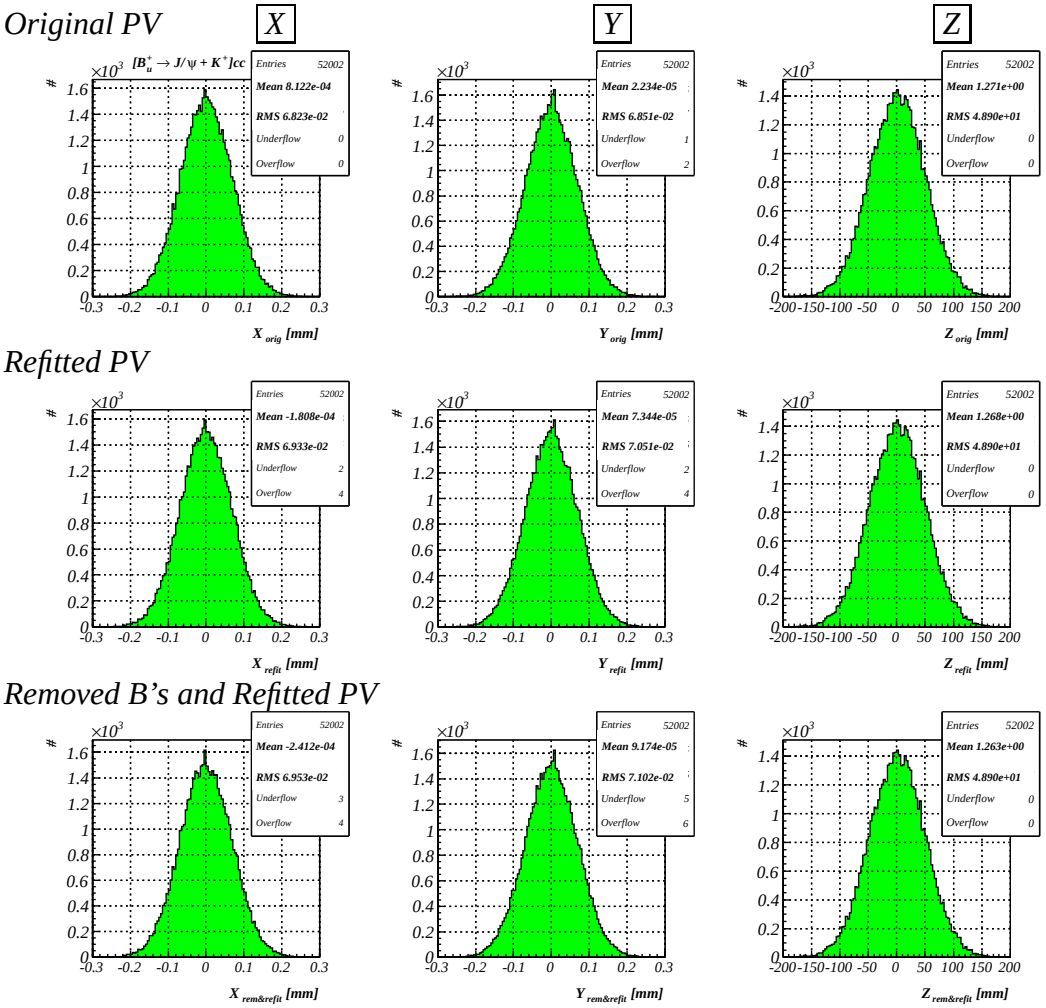

Figure 27: *Distributions of the coordinates of the Primary Vertex, X, Y and Z for the 3 considered cases: Non updated PV, Only refitted PV and Updated PV (removed B's and refitted). The decay channel is $B^+ \to J/\psi K^+$.*

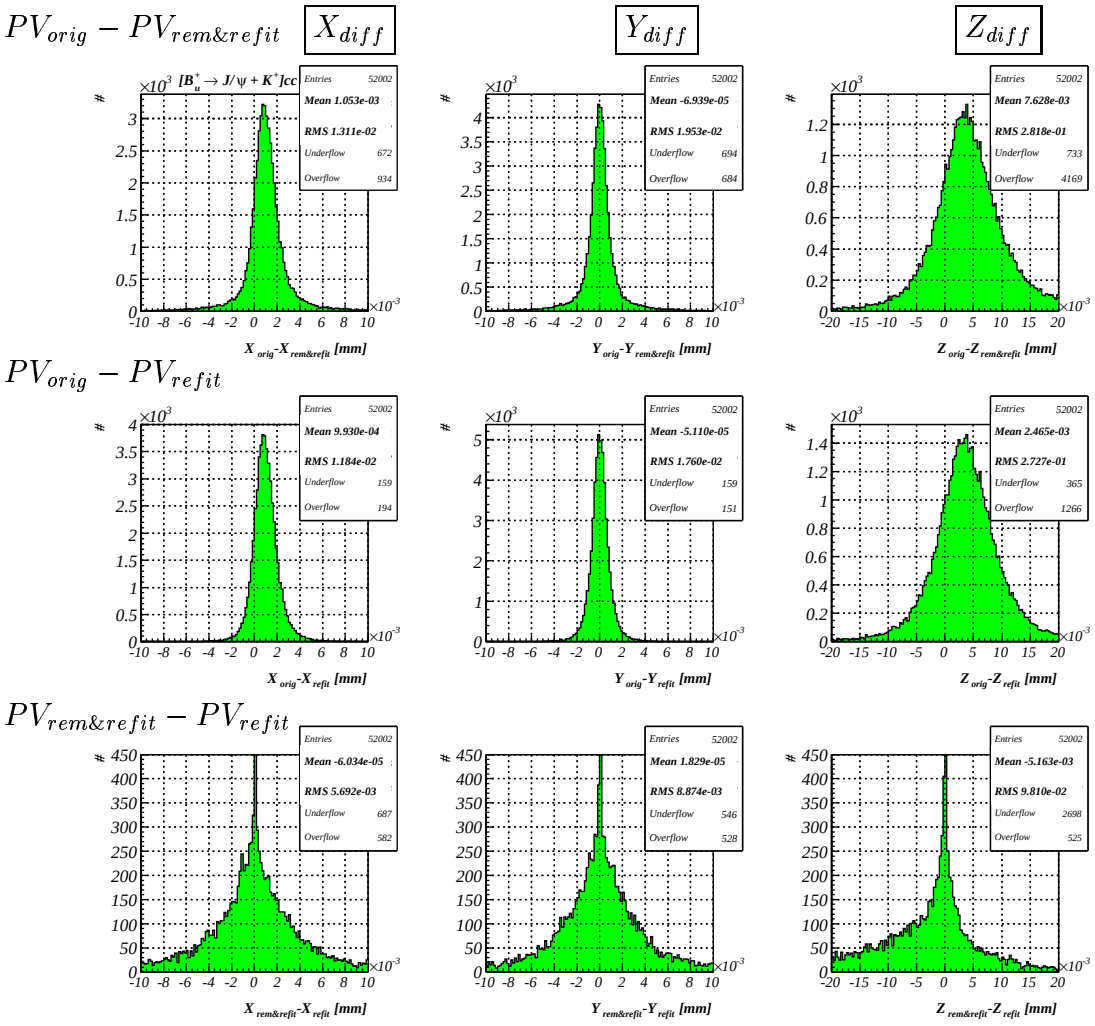

Figure 28: *Distributions of the Primary Vertex X, Y and Z differences $[PV_{orig} - PV_{rem\&refit}]$, $[PV_{orig} - PV_{refit}]$ and $[PV_{rem\&refit} - PV_{refit}]$. The decay channel is $B^+ \rightarrow J/\psi K^+$. (The mean and RMS in the statistics box are not taken from the histogram, but were calculated on an event-by-event basis.)*

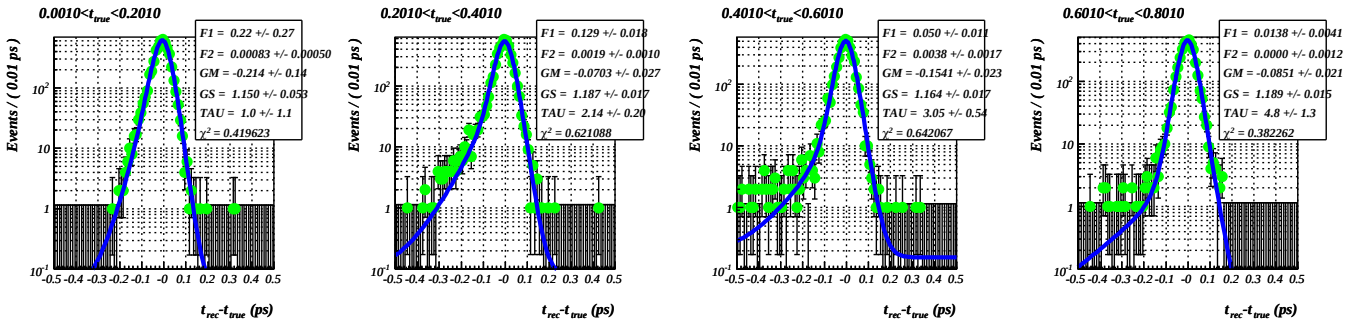

Figure 29: *Original, nominally reconstructed PV. Projections of the unbinned maximum likelihood fits to the* $[t_{rec} - t_{true}]$ *axis for the corresponding slices of* t_{true} *for* $B^+ \to J/\psi K^+$.

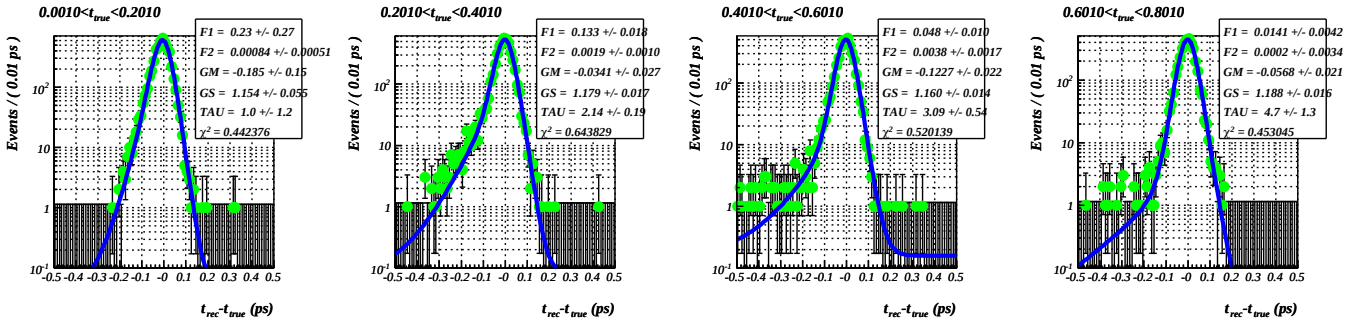

Figure 30: *Refitted only PV. Projections of the unbinned maximum likelihood fits to the* $[t_{rec} - t_{true}]$ *axis for the corresponding slices of* t_{true} *for* $B^+ \to J/\psi K^+$.

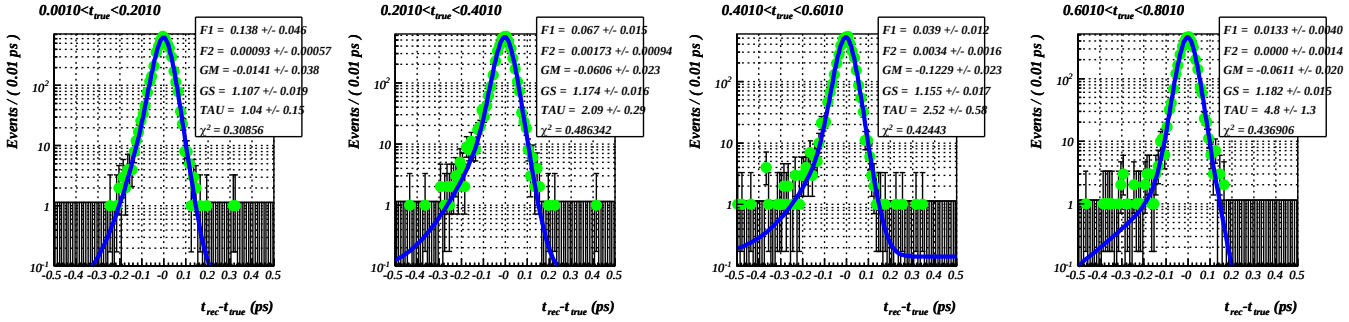

Figure 31: *Removed* B *associates and refitted PV. Projections of the unbinned maximum likelihood fits to the* $[t_{rec} - t_{true}]$ *axis for the corresponding slices of* t_{true} *for* $B^+ \to J/\psi K^+$.

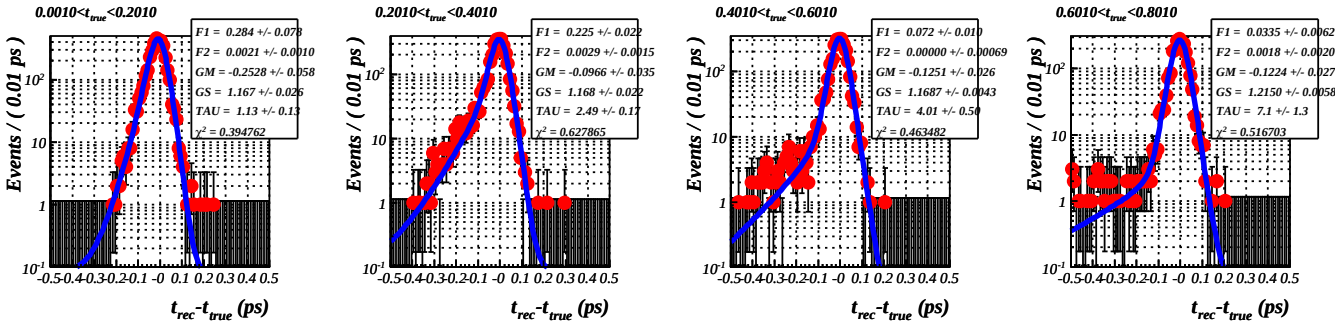

Figure 32: *Original, nominally reconstructed PV. Projections of the unbinned maximum likelihood fits to the* $[t_{rec} - t_{true}]$ *axis for the corresponding slices of* t_{true} *for* $B^0 \to J/\psi K^*$.

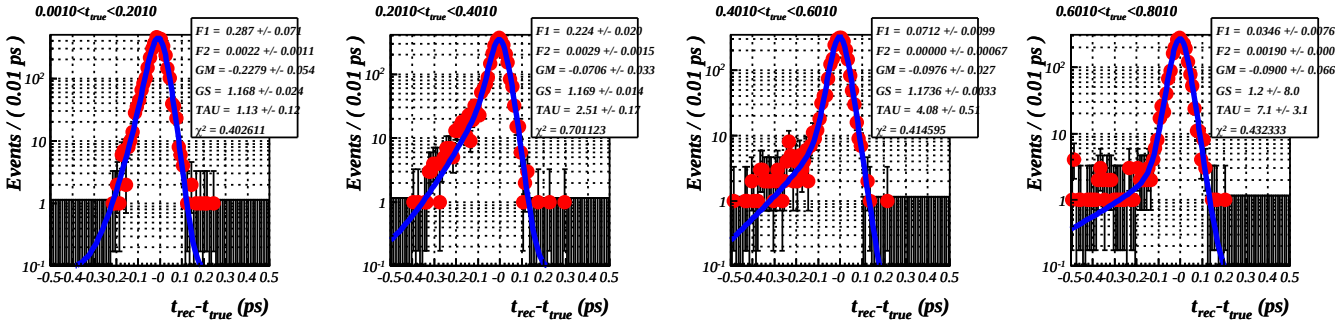

Figure 33: *Refitted only PV. Projections of the unbinned maximum likelihood fits to the* $[t_{rec} - t_{true}]$ *axis for the corresponding slices of* t_{true} *for* $B^0 \to J/\psi K^*$.

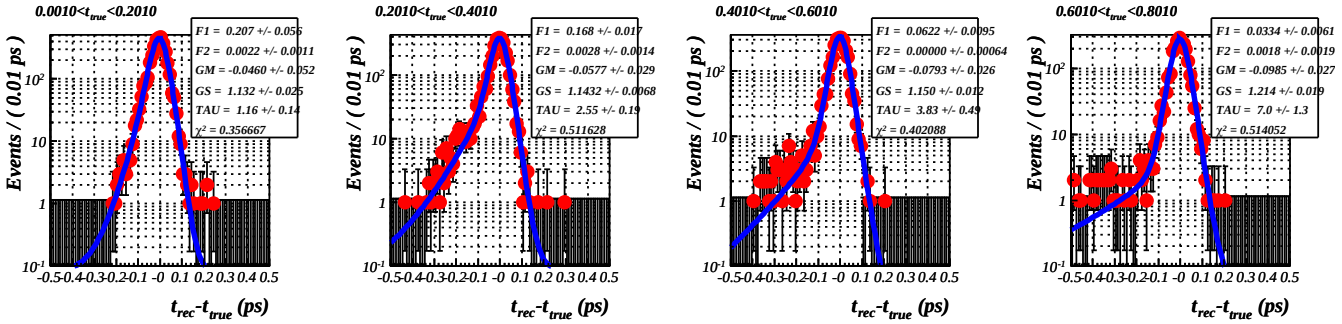

Figure 34: *Removed* B *associates and refitted PV. Projections of the unbinned maximum likelihood fits to the* $[t_{rec} - t_{true}]$ *axis for the corresponding slices of* t_{true} *for* $B^0 \to J/\psi K^*$.

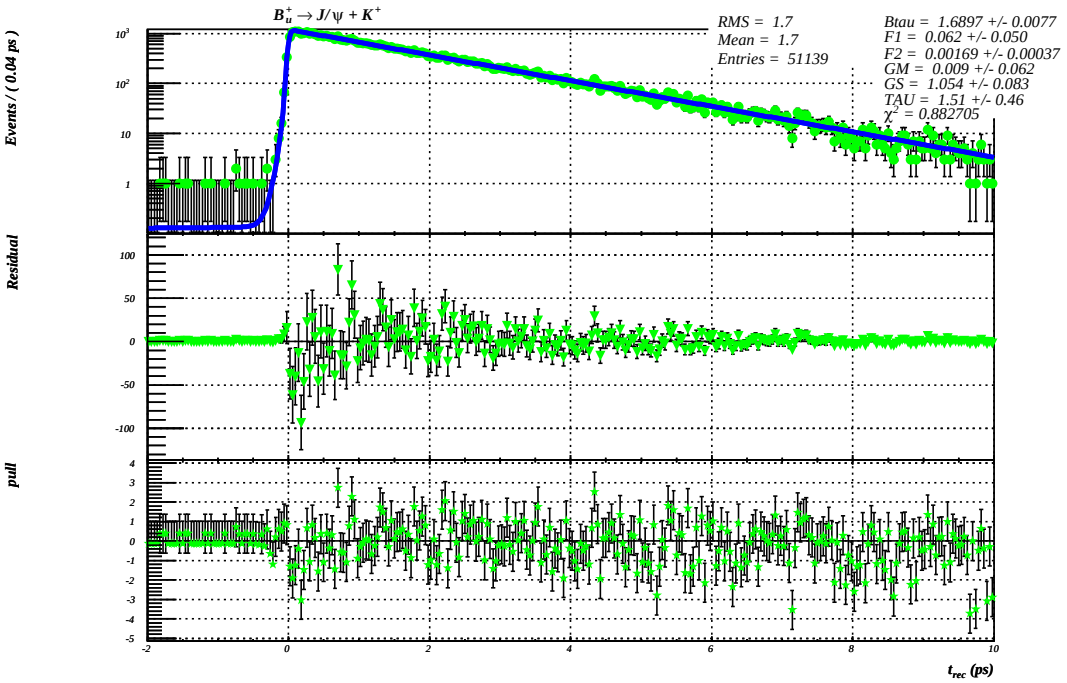

Figure 35: *Projection of the global-unbinned fit to t_{rec} for channel $B^+ \to J/\psi(1S)K^+$ with updated PV. Fit residuals and pulls are given also.*

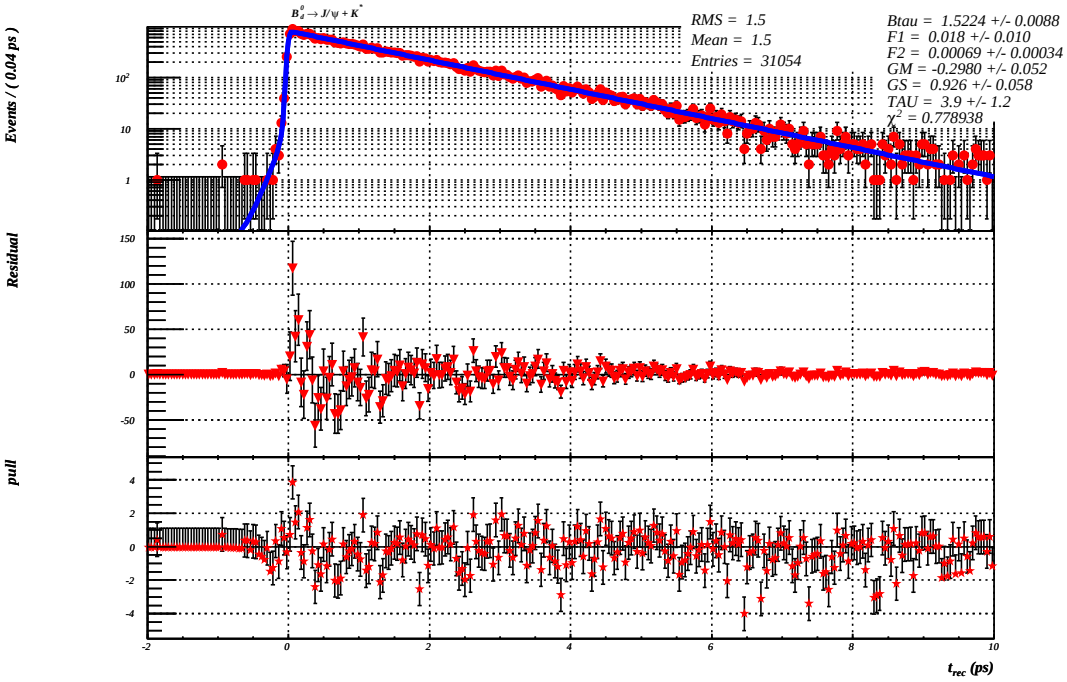

Figure 36: *Projection of the global-unbinned fit to t_{rec} for channel $B^* \to J/\psi(1S)K^*$ with updated PV. Fit residuals and pulls are given also.*

6.3.1 The resolution model parameters after the update of the PV

In Table 5 and Table 6 the resolution model parameters are listed from the global unbinned maximum likelihood fits to the decay time residuals and to t_{rec}, given $\sigma_{t_{rec}}$ for a non-updated nominally reconstructed PV and for a re-defined PV with the B particles removed for $B^+ \to J/\psi K^+$ decay mode. Note that Table 5(7) gives the same results as Table 3 (4), with the only difference that the data set used in Table 5(7) is a factor 2 smaller.

Parameter	Fit to $(t_{rec} - t_{true})$ $[\vec{p}_{resid}]$	Error	Fit to t_{rec} $[\vec{p}_{t_{rec}}]$	Error	Global Correlation Factor
τ_{B^+}			1.6945	0.0072	0.1761
F1	0.0434	0.0058	0.2537	0.3180	0.9978
F2	0.0015	0.0003	0.0015	0.0004	0.3920
GM	-0.1007	0.0076	-0.1509	0.1680	0.9683
GS	1.1700	0.0051	0.5988	0.0937	0.9024
TAU	1.7785	0.1390	1.0071	13.2000	0.9968

Table 5: *Resolution model parameters with nominally reconstructed, original, PV for* $B^+ \to J/\psi K^+$.

Parameter	Fit to $(t_{rec} - t_{true})$ $[\vec{p}_{resid}]$	Error	Fit to t_{rec} $[\vec{p}_{t_{rec}}]$	Error	Global Correlation Factor
τ_{B^+}			1.6897	0.0077	0.2172
F1	0.0381	0.0073	0.0617	0.0503	0.9714
F2	0.0015	0.0003	0.0017	0.0004	0.1201
GM	-0.0517	0.0082	0.0094	0.0620	0.7364
GS	1.1598	0.0054	1.0536	0.0827	0.8524
TAU	1.5330	0.1540	1.5117	0.0456	0.9453

Table 6: *Resolution model parameters with updated PV for* $B^+ \to J/\psi K^+$.

When the PV is updated, removing the B tracks from its reconstruction (Tab. 6), then the matching of the two sets of parameters (from the fit to $(t_{rec} - t_{true})$ and from the fit to t_{rec}) is significantly better in comparison with the case of using the nominal PV (Tab. 5). In fact all the parameters agree well, with the exception of *GM*. A reason for this could be that the t_{true} dependence effect is not fully overcome and still partially present.
The results for the global parameters for a non-updated and updated primary vertex for channel $B^0 \to J/\psi K^*$ are summarized in Table 7 and Table 8. Here we

do not observe as clear improvement of the parameters values. The values of the most important parameters *GS* and *TAU* agree within the errors, but *GM*, *F1* and *F2* are not getting closer.

Parameter	Fit to $(t_{rec} - t_{true})$ $[\vec{p}_{resid}]$	Error	Fit to t_{rec} $[\vec{p}_{t_{rec}}]$	Error	Global Correlation Factor
τ_{B^0}			1.5224	0.0088	0.1709
F1	0.0575	0.0059	0.0305	0.0162	0.9326
F2	0.0032	0.0006	0.0007	0.0004	0.2907
GM	-0.1237	0.0094	-0.4398	0.0465	0.4703
GS	1.2054	0.0067	0.7214	0.0541	0.6637
TAU	2.5331	0.1700	3.1721	0.8970	0.9164

Table 7: *Resolution model parameters with nominally reconstructed, original PV for* $B^0 \to J/\psi K^*$.

Parameter	Fit to $(t_{rec} - t_{true})$ $[\vec{p}_{resid}]$	Error	Fit to t_{rec} $[\vec{p}_{t_{rec}}]$	Error	Global Correlation Factor
τ_{B^0}			1.5224	0.0088	0.1869
F1	0.0458	0.0043	0.0183	0.0101	0.9148
F2	0.0031	0.0006	0.0007	0.0003	0.2363
GM	-0.0744	0.0087	-0.2981	0.0515	0.4859
GS	1.1942	0.0063	0.9261	0.0579	0.6438
TAU	2.6206	0.1870	3.9468	1.1900	0.8989

Table 8: *Resolution model parameters with updated PV for* $B^0 \to J/\psi K^*$

To quantify the goodness of matching of the two sets of parameters ($\vec{p}_{resid}$ and $\vec{p}_{t_{rec}}$), one can compute the following χ^2:

$$\chi^2(\vec{\alpha}) = \vec{\alpha}^T (\mathrm{Cov}_{\vec{\alpha}})^{-1} \vec{\alpha} \ , \tag{20}$$

where

$$\vec{\alpha} = \vec{p}_{resid} - \vec{p}_{t_{rec}} \ , \tag{21}$$

$$\mathrm{Cov}_{\vec{\alpha}} = \mathrm{Cov}_{\vec{p}_{resid}} + \mathrm{Cov}_{\vec{p}_{trec}} \ , \tag{22}$$

with $\mathrm{Cov}_{\vec{p}_{resid}}$ and $\mathrm{Cov}_{\vec{p}_{trec}}$ the covariance matrices of $\vec{p}_{resid}$ and $\vec{p}_{t_{rec}}$ respectively. Table 9 presents the calculated values of $\chi^2/n.d.o.f.$ and the corresponding probabilities, for nominal and updated PV for both channels.

channel	Nominal PV		Updated PV	
	χ^2/n.d.o.f.	*probability*	χ^2/n.d.o.f.	*probability*
$B^+ \to J/\psi K^+$	128/5	0	5.67/5	0.34
$B^0 \to J/\psi K^*$	173/5	0	69/5	$2 \cdot 10^{-13}$

Table 9: χ^2 *values, Eq. (20) and the corresponding probabilities, characterizing the goodness of matching of* $\vec{p}_{resid}$ *and* $\vec{p}_{t_{rec}}$ *for nominal and updated PV for both channels.*

It is clear that the level of consistency of the parameters $\vec{p}_{resid}$ and $\vec{p}_{t_{rec}}$ is strongly increased when the PV is updated. In particular, for the B^+ decay mode, we achieve a χ^2/n.d.o.f. $= 1.1$ corresponding to a χ^2-probability of 34%.
For the B^0 channel the agreement between the determined parameter values is also improved. However, the agreement obtained is still not at the desired level.

7 Summary and conclusions

A proper time resolution model was derived using simulated data. The parameters of this model have been extracted in two ways: using the known residuals in the simulated data, and using the reconstructed proper time only. The latter can be used to determine the parameters of the model in real data. The parameter values obtained in both scenarios were compared.
A discrepancy was found in the values of the resolution model parameters obtained from these two techniques. This is explained as the result of a bias on the reconstructed proper-time which depends on the true proper-time. This bias can be decreased considerably when all final state tracks from the B meson under consideration are explicity removed from the primary vertex, but it is not yet fully resolved.
The method demonstrated here has two potential applications in LHCb: firstly, it could be used for tuning the Monte-Carlo itself; and secondly, for its principal intended purpose, of determining the proper-time resolution parameters on real data.

References

[1] *"LHCb Reoptimized Detector Design and Performance"*, CERN/LHCC 2003-030, LHCb TDR 9, 09.09.2003.

[2] I. Belyaev et al. *"Simulation for the LHCb experiment"*, arXiv:physics/0306035, 2003

[3] *"The BOOLE Project"*, http://lhcb-release-area.web.cern.ch/LHCb-release-area/DOC/boole/

[4] *"The BRUNEL Project"*, http://lhcb-release-area.web.cern.ch/LHCb-release-area/DOC/brunel/

[5] *"The DAVINCI Project"*, http://lhcb-release-area.web.cern.ch/LHCb-release-area/DOC/davinci/

[6] G. Raven *"Selection of $B_s \to J/\psi\phi$ and $B^+ \to J/\psi K^+$"*, LHCb 2003-118

[7] K. Cranmer *"Kernel estimation in High-Energy Physics"*, hep-ex/0011057

[8] W. Werkerke, D. Kirkby *"The RooFit ToolKit for Data Modelling"*, http://roofit.sourceforge.net/

[9] R. Burn, F. Rademakers *"An Object-Oriented Data Analysis Framework"*, http://root.cern.ch/